

Synthesis and Evaluation of Agelastatin Derivatives as Potent Modulators for Cancer Invasion and Metastasis

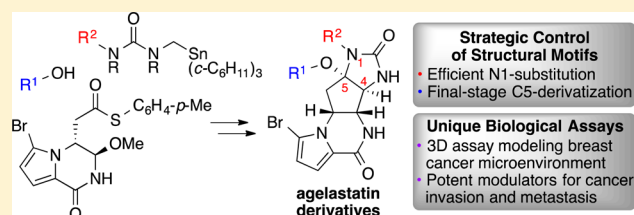
Alyssa H. Antropow,[†] Kun Xu,[‡] Rachel J. Buchsbaum,^{‡,§} and Mohammad Movassaghi^{*,†}

[†]Department of Chemistry, Massachusetts Institute of Technology, Cambridge, Massachusetts 02139, United States

[‡]Molecular Oncology Research Institute and [§]Department of Medicine, Tufts Medical Center, Boston, Massachusetts 02111, United States

Supporting Information

ABSTRACT: The synthesis of new agelastatin alkaloid derivatives and their anticancer evaluation in the context of the breast cancer microenvironment is described. A variety of N1-alkyl and C5-ether agelastatin derivatives were accessed via application of our strategy for convergent imidazolone synthesis from a common thioester along with appropriately substituted urea and alcohol components. These agelastatin derivatives were evaluated in our three-dimensional coculture assay for the effects of mammary fibroblasts on associated breast cancer cells. We have discovered that agelastatin alkaloids are potent modulators for cancer invasion and metastasis at noncytotoxic doses. Herein, we discuss the increased potency of (–)-agelastatin E as compared to (–)-agelastatin A in this capacity, in addition to identification of new agelastatin derivatives with activity that is statistically equivalent to (–)-agelastatin E. The chemistry described in this report provides a platform for the rapid synthesis of agelastatin derivatives with excellent potency (50–100 nM) as modulators for cancer invasion and metastasis.



INTRODUCTION

The agelastatin alkaloids¹ have been of interest to the scientific community for many years due to their intriguing molecular structure as well as potent biological activities.² Our group has reported a general strategy for the total synthesis of all known (–)-agelastatins (1–6, Figure 1), thus enabling the compre-

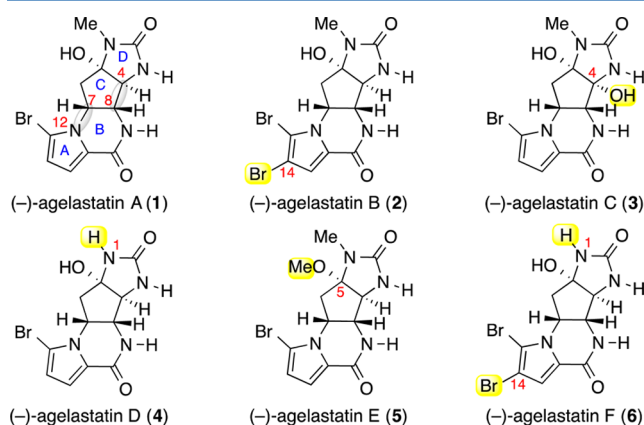


Figure 1. Structures of (–)-agelastatins A–F (1–6).

hensive, comparative anticancer study of these naturally occurring alkaloids along with many synthetic derivatives.³ Distinct from prior approaches to the synthesis of agelastatins,⁴ our strategy employs late-stage C-ring formation with concomitant introduction of three stereocenters.³ Recent work in this area has offered new synthetic strategies⁵ as well

as biological study of the natural alkaloids and synthetic derivatives.⁶ Critical to the success of our unified chemical synthesis of agelastatins was the development of a methodology for the direct conversion of a common thioester to the corresponding imidazolone that serves as a nucleophile in a biogenetically inspired cyclization event to secure the CD-ring portion of these alkaloids. In addition to streamlining our synthesis of all known agelastatin alkaloids, this strategy provides the foundation for access to various derivatives.^{3,7} Our synthesis enables late-stage diversification to two series of agelastatin derivatives with variations at the N1- and C5-positions of the agelastatin core, respectively. Herein we discuss the synthesis of these agelastatin derivatives and their evaluation along with natural agelastatins in a three-dimensional (3D) coculture assay to determine their impact on fibroblasts in the tumor microenvironment.^{8,9} Furthermore, we describe our discovery of the increased potency of (–)-agelastatin E (5, AgE, Figure 1) and distinct new derivatives as compared to (–)-agelastatin A (1, AgA, Figure 1) as modulators for cancer invasion and metastasis.

Previously, we have shown that AgA (1, Figure 1) at concentrations well below the cytotoxic range inhibits vitamin D-induced transcription of osteopontin (OPN) in mammary fibroblasts.⁹ In this setting, OPN transcription and secretion is induced by down-regulation of the Rac GTPase exchange factor Tiam1.¹⁰ Down-regulation of fibroblast Tiam1 and up-regulation of fibroblast OPN in the tumor microenvironment

Received: May 12, 2017

Published: July 11, 2017

are associated with increased invasiveness in human breast cancers.⁹ We have developed a method of 3D coculture enabling assessment of the effects of mammary fibroblasts on associated breast cancer cells.⁸ This has led to the finding that the mammary fibroblast Tiam1-OPN pathway modulates breast cancer invasion and metastasis by regulating epithelial-mesenchymal transition (EMT) and cancer stem cell populations in associated breast cancer cells.^{9,11} The concentrations of AgA (1) in the aforementioned assays (75–100 nM) are far below the cytotoxic range in cell culture. However, we found that direct dosing of mice with AgA (1) at the previously published *in vivo* dose used in 1–4 day studies^{1c,2b,d} (2.5 mg/kg/day) led to toxicity in the animals within 3–4 weeks that precluded further dosing.¹² We therefore sought to determine whether related compounds would have similar or enhanced potency compared with AgA (1).

RESULTS AND DISCUSSION

Synthesis of New Agelastatin A and E Derivatives. In addition to studying other natural members of the agelastatin alkaloid family, we sought to examine new agelastatin derivatives in our 3D coculture assay modeling the breast cancer microenvironment.⁸ Prompted by our preliminary biological data, we were particularly interested in accessing two types of derivatives arising from late-stage modifications to our strategy for synthesis of agelastatins.³ As illustrated in Figure 2, the AgE derivative series 7 includes C5-ether variants

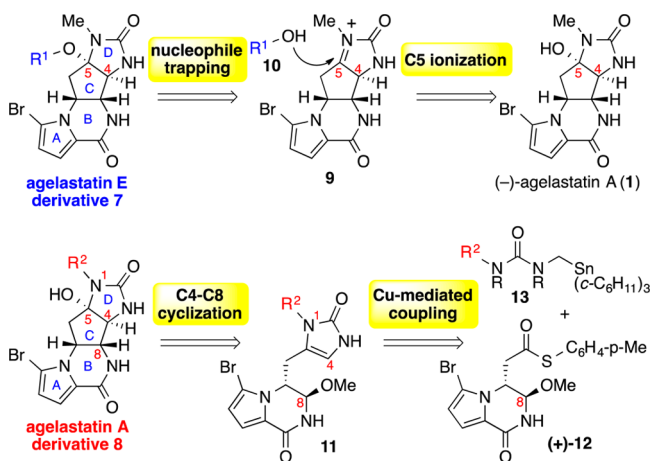


Figure 2. Retrosynthetic analysis of agelastatin alkaloid derivatives.

that were envisioned to be prepared by nucleophilic trapping of iminium ion 9, consistent with our reported preparative conditions for the conversion of AgA (1) to AgE (5).^{3a} Complementarily, the AgA derivative series 8 (Figure 2) includes N1-substituted analogues that were designed to be accessed via application of our imidazolone D-ring synthesis methodology. Starting with thioester (+)-12 and substituted urea 13, we envisioned rapid access to N1-substituted preagelastatin 11 as the substrate for our C-ring cyclization reaction.³ We sought to introduce functional handles for diversification of agelastatin alkaloids while maintaining the newly discovered potency in breast cancer microenvironments.

We have prepared numerous agelastatin alkaloid derivatives (Table 1) through application of our methodology for the synthesis of preagelastatin 11 that is subject to C-ring cyclization followed by C5-substitution. Under our optimal conditions (*vide infra*), C5-ionization of AgA (1) followed by

Table 1. N1- and C5-Substituted Agelastatin Derivatives Prepared for This Study

entry	substituent	agelastatin derivative
agelastatin E derivatives $R^2 = \text{Me}$		
R^1X		
1		7a
2		7b
3		7c
4		7i, $n = 1$
5		7d, $n = 2$
6		7e, $n = 1$
7		7f, $n = 2$
8		7g, $n = 1$
9		7h, $n = 2$
10		7j, $R = \text{Me}$
11		7k, $R = \text{Ph}$
agelastatin A derivatives $R^1X = \text{OH}$		
R^2		
12		8a, $n = 1$
13		8b, $n = 3$
14		8c
15		8d
16		8e, $R^1X = \text{N}_3$
agelastatin derivative		
17		14

nucleophilic trapping afforded the C5-substituted AgE derivative series 7 (Table 1, entries 1–11). Our versatile imidazolone synthesis methodology using the common thioester (+)-12 allowed for introduction of the N1 substituent in preagelastatin 11, which after cyclization afforded the desired N1-substituted AgA derivative series 8 (Table 1, entries 12–16). These new compounds offer diverse functional groups enabling additional derivatization with potential for future studies concerning agelastatin alkaloids. Importantly, our synthesis of agelastatin derivatives 7 and 8 was informed and guided by our concurrent biological studies of these alkaloids. Specifically, our biological evaluation of AgA (1) and AgE (5) disclosed herein has been critical to the design and synthesis of our agelastatin derivatives including those illustrated in Table 1.

Studies of AgE in Breast Cancer Microenvironments.

In the aforementioned 3D assay system, AgA (1) at low concentrations abrogates the effects of up-regulated fibroblast OPN on cancer cell adhesion, invasion, and cancer stem cell populations. Cancer cells exposed in coculture to fibroblasts with up-regulated OPN demonstrated increased levels of lung metastasis in murine xenograft models, which were completely blocked by AgA (1) treatment of the cocultures.⁹ Given our interest in examining other agelastatins for their activity in blocking vitamin D-induced OPN transcription in fibroblasts, we first examined the other natural members of the agelastatin alkaloid family, (–)-agelastatins B–F (2–6, Figure 1), prepared in our previous synthetic studies.³ In our preliminary studies, we only found AgA (1) and AgE (5) to have the desired activity, suggesting a possible negative influence of N1-dealkylation (AgD and AgF), C4-hydroxylation (AgC), or C14-bromination (AgB and AgF) of the agelastatin core. In initial experiments testing effects on cell proliferation, we confirmed that none of the natural agelastatin alkaloids induced cytotoxicity over a range of concentrations (25–250 nM). Given the duration of the 3D cocultures and biologic assays, we specifically aim to use these compounds at noncytotoxic concentrations. (–)-Agelastatins B–F (2–6) all have similar effects on cell viability, and even up to 250 nM concentration, none of these compounds suppress proliferation to a greater extent than AgA (1) at 100 nM concentration.¹³ In dose-response experiments in two-dimensional (2D) cultures, we have previously demonstrated that treatment with 100 nM AgA (1) results in maximal suppression of vitamin D-induced increase in OPN transcription.⁹ Interestingly our screening of the natural agelastatin alkaloids revealed that AgE (5) consistently blocked stimulated OPN transcription and demonstrated increased potency (Figure 3) in comparison to AgA (1), prompting future examination of new C5-substituted agelastatins in this context.

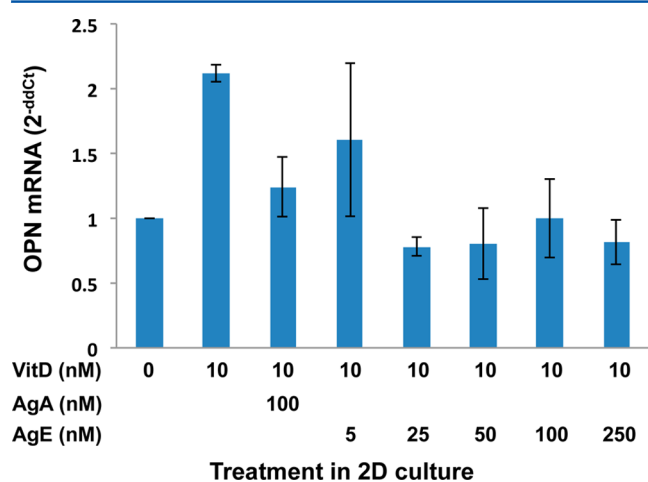


Figure 3. AgE (5) blocks stimulated transcription of osteopontin in fibroblasts. VitD = vitamin D.

Furthermore, we tested the efficacy of AgE (5) in blocking the effects of up-regulated fibroblast OPN in 3D cocultures with the breast cancer cell line SUM1315. Cancer cells were cocultured in 3D media mixture with reduction mammary fibroblasts (RMF) with either wild-type retroviral hairpin control vector (C-RMF) or Tiam1 silencing hairpin vector (shTiam-RMF). While both control and Tiam1-deficient

fibroblasts secrete OPN to some degree, fibroblasts with Tiam1 silencing have up-regulated OPN.⁹ Cocultures were treated with dimethyl sulfoxide (DMSO), AgA (1) at 75 nM concentration, or AgE (5) at 25 or 50 nM concentration. The reference concentration (75 nM) for AgA (1) in 3D coculture assays was determined on the basis of extensive prior biologic and in vivo testing over a range of concentrations, including demonstrated lack of toxicity against all cell lines used in the 3D cocultures.⁹

In the cocultures, fibroblasts and breast cancer cells aggregate to form spheres, with the fibroblasts forming the interior core and the cancer cells on the exterior.¹¹ SUM1315 is an aggressive breast cancer cell line, and under these conditions, the cancer cells form multicellular projections extending out into the 3D matrix, with the number and/or length of the projections indicating degree of invasiveness. Coculture with Tiam1-deficient fibroblasts promotes increased invasiveness, consistent with increased OPN secretion, seen as increased numbers of projections per sphere (Figure 4, column 5) as

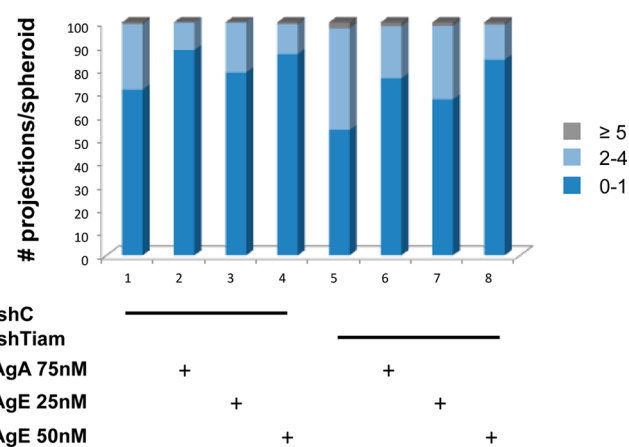


Figure 4. Effect of AgA (1) and AgE (5) on breast cancer cell invasion in cocultures with mammary fibroblasts. Number of projections per spheroid for SUM1315 breast cancer cells and indicated mammary fibroblasts in 3D mixed cell spheroid coculture is shown as percent of total spheroids. shC = control silencing retroviral hairpin vector. shTiam = Tiam1 silencing hairpin vector.

compared to control fibroblasts (Figure 4, column 1). Incorporation of AgA (1) at 75 nM concentration with Tiam1-deficient fibroblasts (Figure 4, column 6) decreased the number of projections to the baseline number seen with control fibroblast coculture (Figure 4, column 1). Furthermore, including AgE (5) at 25 nM concentration (Figure 4, column 7) partially decreased the number of projections toward baseline, while AgE (5) at 50 nM concentration (Figure 4, column 8) reduced the number of projections to below the baseline condition. Excitingly, these results suggest that AgE (5) is more potent than AgA (1) in decreasing the invasiveness induced by Tiam1-deficient fibroblasts.

For further assessment, we isolated the breast cancer cells from the 3D cocultures to greater than 99% purity as described previously.^{8,10} Adhesion of these postcoculture (PCC) cells was assessed through transwell migration assay (Figure 5). As with the invasion assay results, migration was notably increased in PCC cells exposed to Tiam1-deficient fibroblasts (Figure 5, column 5) compared with PCC cells exposed to control fibroblasts (Figure 5, column 1). This increased migration was blocked by incorporation of AgA (1) at 75 nM concentration in

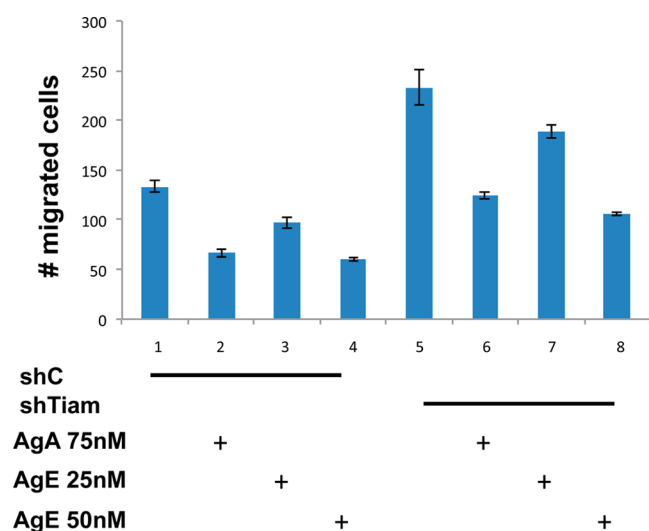


Figure 5. Effect of AgE (5) on migration potential of breast cancer cells isolated from coculture with mammary fibroblasts.

the cocultures (Figure 5, column 6). Significantly, including AgE (5) at 25 and 50 nM concentrations (Figure 5, columns 7 and 8) also decreased the migration, with the 50 nM treatment decreasing the number of migrating cells below the baseline condition.

Two assays for breast cancer stem cell populations include tumorsphere formation in low adherence culture conditions and flow cytometry for specific cell surface markers (CD44⁺/CD24⁻/ESA⁺). Results of both assays on the PCC cells showed analogous findings to the aforementioned invasion and migration assays. Incorporation of AgA (1) at 75 nM concentration completely blocked the increased numbers of tumorspheres (Figure 6, column 6) or cancer stem cells (Figure

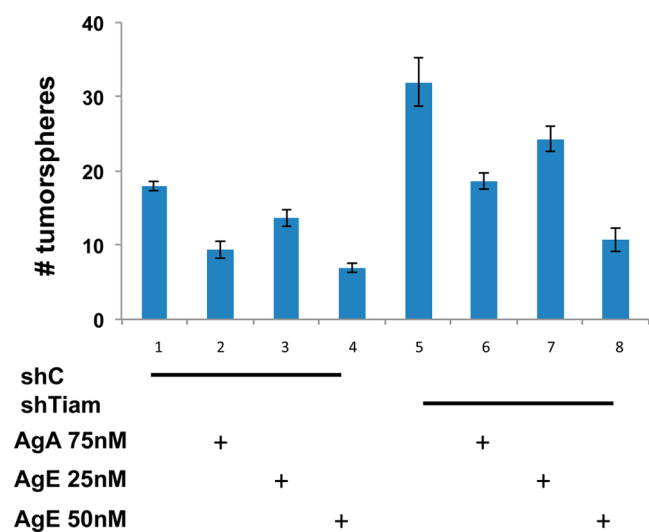


Figure 6. Effect of AgA (1) and AgE (5) on tumorsphere formation by breast cancer cells isolated from coculture with mammary fibroblasts.

7, column 6) induced by Tiam1-deficient fibroblasts, compared with control fibroblasts (Figures 6 and 7, column 1). Incorporation of AgE (5) at 25 nM concentration had a partial effect (Figures 6 and 7, column 7), while AgE (5) at 50 nM concentration decreased tumorsphere and cancer stem cell numbers below baseline (Figures 6 and 7, column 8).

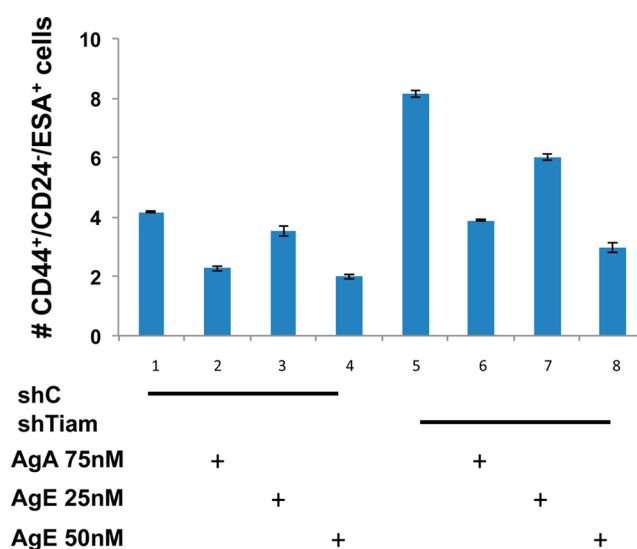


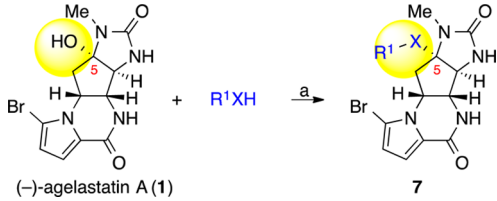
Figure 7. Effect of AgA (1) and AgE (5) on CD44⁺/CD24⁻/ESA⁺ populations in breast cancer cells isolated from coculture with mammary fibroblasts.

Significantly, these results consistently suggest that AgE (5) is more potent than AgA (1) in blocking the effects of fibroblast OPN on the invasiveness, migration potential, and cancer stem cell populations in associated breast cancer cells.

With our increased understanding of the effects of the agelastatin alkaloids in breast cancer microenvironments, particularly the observation that AgE (5) showed increased potency as compared to AgA (1), we sought to prepare the two series of agelastatin derivatives illustrated in Table 1 and study their biological effects on breast cancer invasiveness.

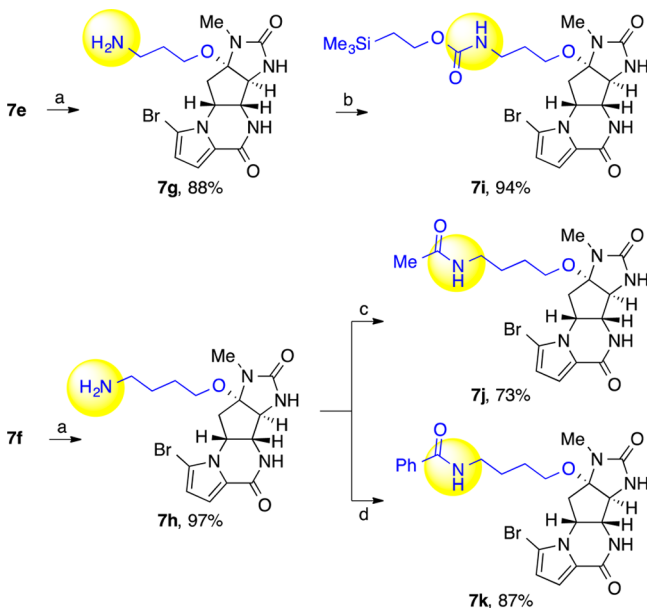
Development of Agelastatin E Derivatives. We envisioned the preparation of AgE derivative series 7 would require conditions similar to those we developed for the direct conversion of the C5-hydroxy group of AgA (1) to the C5-methoxy group of AgE (5).^{3a} In the event, treatment of AgA (1) with methanesulfonic acid to promote the formation of C5-iminium ion 9 (Figure 2) followed by in situ trapping with a series of nucleophiles afforded the agelastatin derivatives 7a–f (Table 2). Condensation of commercially available 3-buten-1-ol and 3-buten-1-ol with AgA (1) provided the desired derivatives 7a and 7b, respectively (Table 2, entries 1 and 2). The use of 3-mercaptopropiophenone¹⁴ as the nucleophile afforded the C5-sulfide derivative 7c (Table 2, entry 3). The carbamate derivative 7d was prepared using the corresponding trimethylsilyl ethoxy carbamate-protected 4-aminobutan-1-ol as the nucleophile (Table 2, entry 4). Similarly, the condensation of 3-azidopropan-1-ol and 4-azidobutan-1-ol¹⁵ with AgA (1) resulted in formation of azide derivatives 7e and 7f, respectively (Table 2, entries 5–6). These derivatives provided functional groups amenable to further diversification for use in concurrent biological evaluation.

Azide derivatives 7e and 7f were reduced to the corresponding amines 7g and 7h, respectively, under Staudinger reaction conditions (Scheme 1). The primary amine 7g was converted to carbamate 7i upon treatment with 4-nitrophenyl 2-(trimethylsilyl)ethyl carbonate in the presence of triethylamine. Likewise, primary amine 7h was converted to acetamide 7j and benzamide 7k upon exposure to acetic anhydride and benzoyl chloride, respectively. This subset of AgE derivatives provided compounds with a range of linker

Table 2. Synthesis of AgE derivatives 7a–7f from AgA (1)^{a,b}


entry	R ¹ X	derivative	yield
1		7a	87%
2		7b	68%
3		7c	93%
4		7d	63%
5 ^a		7e, n = 1	74%
6 ^a		7f, n = 2	76%

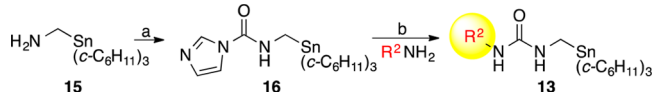
^aCH₂Cl₂ used as solvent. ^bConditions: (a) MeSO₃H, CH₃CN.

Scheme 1. Chemical Diversification of AgE Derivatives 7e–7h^a

^aConditions: (a) PPh₃, THF–H₂O (9:1). (b) 4-nitrophenyl 2-(trimethylsilyl)ethyl carbonate, NEt₃, CH₂Cl₂. (c) Ac₂O, NEt₃, DMAP, THF. (d) BzCl, NEt₃, THF.

lengths along with azide, amine, amide, and carbamate functional groups for our biological evaluation and comparison with AgA (1) and AgE (5) as modulators of breast cancer invasiveness (vide infra).

Development of Agelastatin A Derivatives. The application of our synthetic methodology for the introduction of substituents at the N1 position of agelastatins necessitated the preparation of urea-based organostannane reagent 13 (Table 3).³ The use of substituted urea 13 in our convergent synthesis of substituted imidazolones enabled access to the corresponding N1-substituted preagelastatins en route to the desired AgA derivatives. Through the use of 1,1'-carbon-

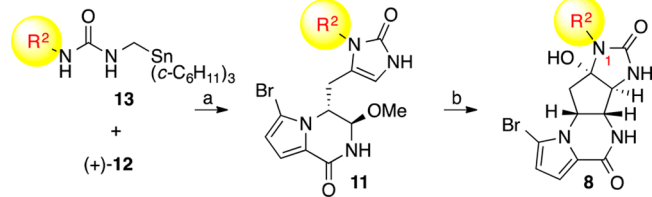
Table 3. Synthesis of Substituted Ureas 13a–c^a


entry	R ²	derivative	yield
1		13a, n = 1	91%
2		13b, n = 3	95%
3		13c	84%

^aConditions: (a) 1,1'-carbonyldiimidazole, DMAP, CH₂Cl₂, 85%. (b) DMAP, CH₂Cl₂, 40 °C.

ylidiimidazole¹⁶ as a phosgene equivalent, we were able to access the versatile intermediate 16 that was converted to substituted ureas 13a–c upon treatment with the desired primary amine (Table 3).^{3,17}

The copper-mediated coupling of substituted urea 13 with versatile thioester (+)-12 directly provided the N1-substituted imidazolone 11 that served as the substrate for our C-ring cyclization chemistry to afford the AgA derivative series 8 (Table 4).³ The use of N1 substituents with a primary alcohol

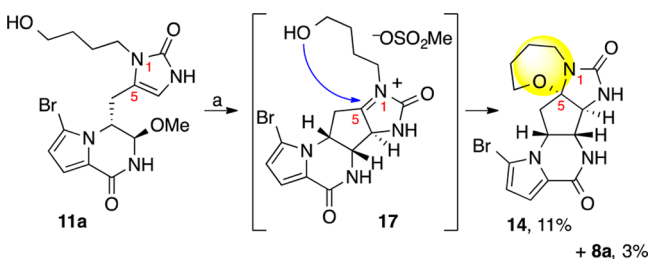
Table 4. Synthesis of AgA Derivatives 8a–c Using Copper-Mediated Coupling^{a,b}


entry	R ²	derivative	yield (11, 8)
1		8a, n = 1	53%, 3% ^a
2		8b, n = 3	67%, 36%
3		8c	61%, 30%

^a8a was isolated along with pentacyclic derivative 14 (11%). ^bConditions: (a) CuTC, THF, 50 °C; HCl, MeOH, 50 °C. (b) MeSO₃H, H₂O, 100 °C. CuTC = copper(I) thiophene-2-carboxylate.

functional group was envisioned to enable postcyclization diversification of the agelastatin core in analogy with the C5 ether series. Preagelastatins 11b and 11c provided modest yield of the corresponding N1-substituted agelastatin derivatives 8b and 8c, respectively (Table 4, entries 2 and 3). Interestingly, the shorter 4-methylene spacer preagelastatin 11a provided the N1-substituted AgA derivative 8a (Table 4, entry 1) along with the pentacyclic agelastatin derivative 14 (Scheme 2). The inefficient formation of agelastatin derivative 8a is likely due to competitive intramolecular trapping of the C5-iminium ion 17 to afford the pentacyclic derivative 14 (Scheme 2). Notably, ether 14 serves as a link between AgE and AgA derivatives, including both N1 and C5 modifications. An anticipated slower rate of intramolecular cyclization using the longer N1 substituents in preagelastatins 11b and 11c is consistent with the observed greater, albeit modest, yield of the corresponding derivatives 8b and 8c, respectively (Table 4).

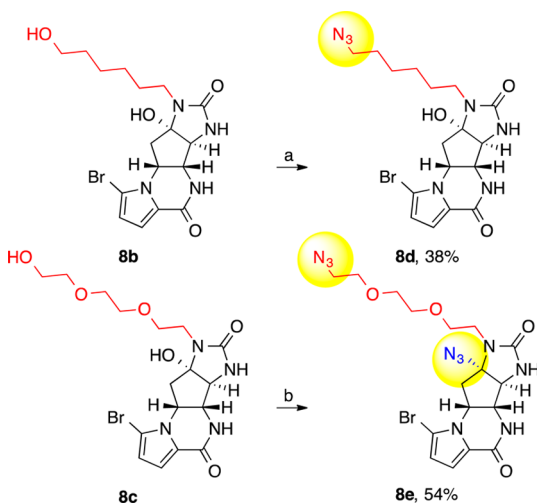
Scheme 2. Observed Double Cyclization of Tricycle 11a to Pentacycle 14^a



^aConditions: (a) MeSO₃H, H₂O, 100 °C.

The primary alcohol of the N1 substituent of AgA derivatives **8a–c** presents an opportunity for introduction of an azide functional group that may be used in the future for further modifications similar to those accomplished in the AgE derivative series **7**. Indeed, using the more readily accessible alcohols **8b** and **8c**, we prepared the corresponding azide derivatives in a single step (Scheme 3). The primary alcohol **8b**

Scheme 3. Chemical Diversification of AgA Derivatives **8b** and **8c** to the Corresponding Azides^a



^aConditions: PPh₃ (n equiv), diisopropylazodicarboxylate (n equiv), diphenyl phosphoryl azide (n equiv), THF. (a) n = 2, **8d** isolated along with 34% recovered starting material. (b) n = 10.

was converted to the agelastatin azide **8d** in 38% yield, along with 34% recovery of the starting material (72% BRSM). When using more forcing conditions required for complete conversion of the more recalcitrant triethylene glycol derivative **8c** to the corresponding azide, we observed the formation of bis-azide **8e** consistent with an additional C5-azidation. Interestingly, mass spectrometric analysis of bis-azide **8e** shows consistency with other AgA derivatives in formation of its corresponding C5-iminium ion as a major observed molecular ion. We were excited to explore bis-azide **8e** in our biological screening conditions, as this is the first example of azide substitution at the C5-position of the agelastatin alkaloids. The covalent linkage of the alcohol and azide functional groups offered in the AgA derivatives **8a–e** was designed to be complementary to the ionizable linkage present in the AgE derivative series **7**.

Biological Study of Agelastatin Alkaloid Derivatives.

As we accessed a variety of agelastatin derivatives as described, we systematically compared them to AgA (**1**) and AgE (**5**) for efficacy in blocking D-induced OPN transcription. The results of these investigations with selected and most informative derivatives are summarized in Figure 8. On the

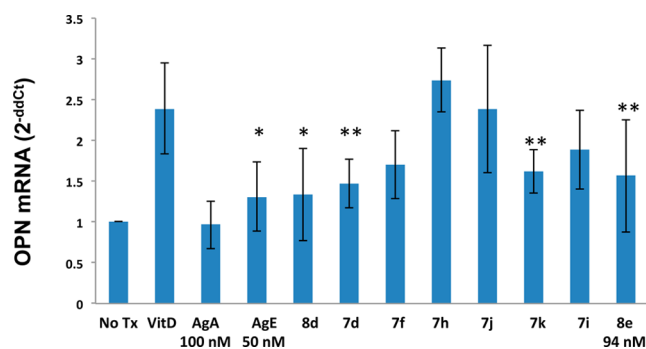


Figure 8. Varying effects of agelastatin derivatives in blocking stimulated fibroblast expression of osteopontin. All agelastatin derivatives were tested at 100 nM concentration unless noted otherwise. *Statistical equivalence with AgA (**1**) at 100 nM concentration; **Equivalence with AgE (**5**) at 50 nM concentration, but not AgA (**1**) at 100 nM concentration by *t* test. No Tx = baseline control with values normalized to transcription of a housekeeping gene.

basis of our prior work with AgA (**1**),⁹ the 100 nM concentration is our standard concentration used for screening large numbers of compounds, which is well within the noncytotoxic range for all natural agelastatin alkaloids in the proliferation assays described above. Furthermore, upon treatment with agelastatin derivatives, all cells were observed to grow at equal rates and require equal handling during passage in culture, indicating similar effects on proliferation and viability.¹⁸ Of particular interest in our initial screens were the AgE derivative carbamate **7d** and the AgA derivative azide **8d**. In further studies of AgA derivatives, the triethylene glycol linked bis-azide **8e** showed improved efficacy in our assays. Indeed, bis-azide **8e** at 94 nM concentration demonstrates statistical equivalence to AgE (**5**) at 50 nM concentration in blocking vitamin D-induced OPN transcription. We designed AgE derivatives **7i–k** (Scheme 1) in an effort to better understand the promising potency of carbamate **7d** in our preliminary assays. Our aim was to differentiate between the aspects of the linker that led to increased potency, such as the electronic properties, steric factors, and linker length. Interestingly, the 4-methylene-linked carbamate **7d** maintained slightly improved potency compared to the related 3-methylene linked carbamate **7i**, consistent with the notion that the linker length is important to maintaining the desired inhibitory activity. While acetamide derivative **7j** maintains the substituent chain length of carbamate **7d**, its comparatively decreased activity suggests that the acetamide group is not as effective as the larger trimethylsilyl ethoxy substituent of carbamate **7d**. Benzamide derivative **7k** excitingly showed the desired potency comparable to carbamate **7d** by preserving the substituent chain length of carbamate **7d** while offering a larger amide group as compared to acetamide **7j**. Notably, these results highlight the notion that both N1- and C5-substitution are not only tolerated in agelastatins with potency in modulation of breast cancer invasiveness, but also have already offered ample

opportunities to access compounds that begin to approach our newly discovered potency of AgE (5) in this context. We envision the chemistry described herein to enable access to a wide range of new synthetic AgA and AgE derivatives as potential modulators of breast cancer invasion and metastasis.

CONCLUSIONS

We demonstrate that (–)-AgE (5) is more potent than (–)-AgA (1) in blocking fibroblast-mediated effects on cancer cell invasion and migration and cancer stem cell populations. Importantly, we have established noncytotoxic doses for the delivery of agelastatin alkaloids to breast cancer microenvironments in order to study their activity in blocking induced OPN transcription in fibroblasts, which can modulate these cancer cell behaviors. Based on the exciting recognition of the potent activity of AgE (5) and AgA (1) in this context, we embarked on the synthesis of a variety of C5- and N1-substituted agelastatin derivatives, culminating in the AgE and AgA derivative series 7 and 8, respectively (Table 1). Highlights of our synthetic strategy include efficient C5 derivatization of AgA (1) using a variety of nucleophiles based on our conversion of AgA (1) to AgE (5),³ selective N1 functionalization using our imidazolone synthesis methodology,³ and diversification of complex agelastatin derivatives and establishment of precedence for access to more complex synthetic derivatives. Furthermore, we demonstrate that our new derivatives 7d and 7k (100 nM concentration) as well as derivative 8e (94 nM concentration) are statistically equivalent to AgE (5) at 50 nM concentration. The chemistry described here provides a foundation for rapid access to agelastatin derivatives with high potency (50–100 nM) as modulators for cancer invasion and metastasis. Our findings highlight the outstanding potential for the development of potent agelastatin derivatives with functional handles for further chemical derivatization and biological applications.

EXPERIMENTAL SECTION

General Methods. All reactions were performed in oven-dried or flame-dried round-bottom flasks. The flasks were fitted with rubber septa, and reactions were conducted under a positive pressure of argon. Cannulae or gastight syringes with stainless steel needles were used to transfer air- or moisture-sensitive liquids. Where necessary (so noted), solutions were deoxygenated by argon purging for a minimum of 10 min. Flash column chromatography was performed as described by Still et al.¹⁹ using granular silica gel (60 Å pore size, 40–63 μm, 4–6% H₂O content). Analytical thin-layer chromatography (TLC) was performed using glass plates precoated with 0.25 mm 230–400 mesh silica gel impregnated with a fluorescent indicator (254 nm). Thin-layer chromatography plates were visualized by exposure to short wave ultraviolet light (254 nm) and irreversibly stained by treatment with an aqueous solution of ceric ammonium molybdate (CAM) or an aqueous solution of potassium permanganate (KMnO₄) or an alcoholic solution of ninhydrin, followed by heating (~1 min) on a hot plate (~250 °C). Organic solutions were concentrated at 29–30 °C on rotary evaporators capable of achieving a minimum pressure of ~2 Torr and then at ~0.5 Torr (vacuum pump) unless otherwise indicated. Proton (¹H) and carbon (¹³C) nuclear magnetic resonance spectra were recorded with 600, 500, and 400 MHz spectrometers. Proton nuclear magnetic resonance (¹H NMR) spectra are reported in parts per million on the δ scale and are referenced from the residual protonium in the NMR solvent [CDCl₃: δ 7.26 (CHCl₃), CD₃OD: δ 3.31 (CD₂HOD), DMSO-*d*₆: δ 2.50 (DMSO-*d*₅)]. Data are reported as follows: chemical shift (multiplicity [s = singlet, d = doublet, t = triplet, q = quartet, m = multiplet], coupling constant(s) in Hertz, integration). Carbon-13 nuclear magnetic resonance (¹³C NMR)

spectra are reported in parts per million on the δ scale and are referenced from the carbon signals of the solvent (CDCl₃: δ 77.16, CD₃OD: δ 49.15, DMSO-*d*₆: δ 39.52). Infrared data (IR) were obtained with a FTIR and are reported as follows: [frequency of absorption (cm⁻¹), intensity of absorption (s = strong, m = medium, w = weak, br = broad)]. High-resolution mass spectrometric data (HRMS) were recorded on a Fourier transform ion cyclotron resonance mass spectrometer (FTICR-MS) using electrospray ionization (ESI) source or direct analysis in real time (DART) ionization source.

General Procedure for Synthesis of AgE Derivatives 7a–f. Methanesulfonic acid (10 equiv) was added slowly to a solution of (–)-agelastatin A (1 equiv) and nucleophile in acetonitrile or dichloromethane. Upon consumption of starting material as shown by thin-layer chromatography, the reaction mixture was diluted with ethyl acetate or dichloromethane as indicated (10 mL). Reactions conducted over molecular sieves were filtered through a plug of cotton and further diluted with the indicated solvent (10 mL). The crude organic mixture was washed sequentially with saturated aqueous sodium bicarbonate solution (2 × 15 mL) and saturated aqueous sodium chloride solution (1 × 10 mL). The combined aqueous layers were extracted with organic solvent (2 × 10 mL). The combined organic layers were dried over anhydrous sodium sulfate, filtered, and concentrated under reduced pressure. The resulting residue was purified by flash column chromatography on silica gel to afford AgE derivatives 7a–f.

Alkyne Derivative 7a. Compound 7a was synthesized according to the general procedure for synthesis of AgE derivatives using 3-butyne-1-ol (0.5 mL) and acetonitrile (2.5 mL) over 4 Å molecular sieves (30 mg). After 17.5 h, the crude residue after workup using ethyl acetate was purified by flash column chromatography on silica gel (eluent: 10% acetone in dichloromethane, then 5% → 10% methanol in dichloromethane) to afford alkyne 7a (10.0 mg, 87%) as a white solid. ¹H NMR (500 MHz, CD₃OD, 23 °C): δ 6.92 (d, *J* = 4.1 Hz, 1H), 6.34 (d, *J* = 4.1 Hz, 1H), 4.62 (dt, *J* = 12.1, 6.0 Hz, 1H), 4.15–4.07 (m, 2H), 3.53–3.44 (m, 1H), 3.38–3.31 (m, 1H), 2.82 (s, 3H), 2.73–2.65 (m, 1H), 2.51–2.44 (m, 2H), 2.32 (t, *J* = 2.7 Hz, 1H), 2.23–2.14 (m, 1H). ¹³C NMR (125 MHz, CD₃OD, 23 °C): δ 161.8, 161.1, 124.2, 116.2, 114.0, 107.5, 99.9, 82.0, 71.0, 62.8, 62.3, 61.8, 53.8, 39.2, 24.9, 20.5. FTIR (thin film) cm⁻¹: 2930 (w), 1667 (s), 1551 (w), 1425 (m), 1098 (w), 747 (w). HRMS (ESI-FTICR) *m/z*: [M + H]⁺ calcd for C₁₆H₁₈BrN₄O₃ 393.0557, found 393.0552. TLC (10% methanol in dichloromethane), *R*_f: 0.69 (UV, CAM).

Alkene Derivative 7b. Compound 7b was synthesized according to the general procedure for synthesis of AgE derivatives using 3-buten-1-ol (0.5 mL) and acetonitrile (2.5 mL) over 4 Å molecular sieves (30 mg). After 18 h, the crude residue after workup using ethyl acetate was purified by flash column chromatography on silica gel (eluent: 10% acetone in dichloromethane, then 5% → 10% methanol in dichloromethane) to afford alkene 7b (8.1 mg, 68%) as a white solid. ¹H NMR (500 MHz, CD₃OD, 23 °C): δ 6.91 (d, *J* = 4.1 Hz, 1H), 6.33 (d, *J* = 4.2 Hz, 1H), 5.93–5.77 (m, 1H), 5.17–5.00 (m, 2H), 4.61 (dt, *J* = 12.2, 5.9 Hz, 1H), 4.11 (d, *J* = 5.4 Hz, 1H), 4.08 (s, 1H), 3.42 (q, *J* = 7.6 Hz, 1H), 3.31–3.21 (m, 1H), 2.78 (s, 3H), 2.66 (dd, *J* = 13.4, 6.5 Hz, 1H), 2.35 (q, *J* = 6.8 Hz, 2H), 2.16 (t, *J* = 12.8 Hz, 1H). ¹³C NMR (126 MHz, CD₃OD, 23 °C): δ 161.9, 161.1, 136.3, 124.2, 117.5, 116.2, 114.0, 107.5, 99.8, 63.8, 62.3, 61.7, 53.8, 39.3, 35.1, 24.9. FTIR (thin film) cm⁻¹: 2926 (w), 1668 (s), 1551 (w), 1425 (m), 1091 (w), 747 (w). HRMS (ESI-FTICR) *m/z*: [M + H]⁺ calcd for C₁₆H₂₀BrN₄O₃ 395.0713, found 395.0692. TLC (10% methanol in dichloromethane), *R*_f: 0.43 (UV, CAM).

Sulfide Derivative 7c. Compound 7c was synthesized according to the general procedure for synthesis of AgE derivatives using 3-mercaptopropiophenone¹⁴ (99.7 mg, 6.00 × 10⁻² μmol, 20.5 equiv) in acetonitrile (3.0 mL) over 4 Å molecular sieves (20 mg). After 1 h, the crude residue after workup using ethyl acetate was purified by flash column chromatography on silica gel (eluent: 0% → 10% methanol in dichloromethane) to afford sulfide 7c (13.6 mg, 93%) as a white solid. ¹H NMR (400 MHz, CD₃OD, 23 °C): δ 8.04–7.94 (m, 2H), 7.65–7.58 (m, 1H), 7.54–7.47 (m, 2H), 6.91 (d, *J* = 4.1 Hz, 1H), 6.32 (d, *J*

= 4.1 Hz, 1H), 4.78 (dt, $J = 11.8, 6.1$ Hz, 1H), 4.47 (s, 1H), 4.19 (d, $J = 5.4$ Hz, 1H), 3.35 (t, $J = 6.9$ Hz, 2H), 2.91 (dd, $J = 12.5, 6.9$ Hz, 1H), 2.87 (s, 3H), 2.81–2.67 (m, 2H), 1.95 (dd, $J = 13.5, 11.7$ Hz, 1H). ^{13}C NMR (100 MHz, CD_3OD , 23 °C): δ 199.7, 161.6, 161.0, 138.0, 134.7, 130.0, 129.3, 124.3, 116.3, 114.1, 107.5, 77.9, 67.5, 63.4, 54.8, 41.0, 38.8, 25.2, 24.1. FTIR (thin film) cm^{-1} : 2920 (w), 2361 (w), 1667 (s), 1551 (w), 1423 (m), 1195 (w). HRMS (ESI-FTICR) m/z : $[\text{M} + \text{H}]^+$ calcd for $\text{C}_{21}\text{H}_{22}\text{BrN}_4\text{O}_3\text{S}$ 489.0591, found 489.0595. TLC (5% methanol in dichloromethane), R_f : 0.46 (UV, CAM).

4-Methylene Carbamate Derivative 7d. Compound **7d** was synthesized according to the general procedure for synthesis of AgE derivatives using 2-(trimethylsilyl)ethyl (4-hydroxybutyl)carbamate²⁰ (1.40×10^2 mg, 6.00×10^2 μmol , 20.5 equiv) in acetonitrile (3.0 mL) over 4 Å molecular sieves (25 mg). After 3 h, the crude residue after workup using ethyl acetate was purified by flash column chromatography on silica gel (eluent: 20% → 30% acetone in dichloromethane, then 5% → 10% methanol in dichloromethane) to afford 4-methylene carbamate **7d** (10.5 mg, 63%) as a white solid. ^1H NMR (400 MHz, CD_3OD , 23 °C): δ 6.89 (d, $J = 4.1$ Hz, 1H), 6.31 (d, $J = 4.1$ Hz, 1H), 4.59 (dt, $J = 12.1, 6.0$ Hz, 1H), 4.17–4.05 (m, 4H), 3.36 (dt, $J = 9.0, 5.8$ Hz, 1H), 3.24 (dt, $J = 9.1, 5.8$ Hz, 1H), 3.08 (td, $J = 6.8, 4.3$ Hz, 2H), 2.76 (s, 3H), 2.68–2.60 (m, 1H), 2.20–2.10 (m, 1H), 1.65–1.49 (m, 4H), 0.99–0.92 (m, 2H), 0.02 (s, 9H). ^{13}C NMR (100 MHz, CD_3OD , 23 °C): δ 161.9, 161.1, 159.5, 124.2, 116.2, 114.0, 107.5, 99.9, 63.9, 63.7, 62.3, 61.7, 53.8, 41.4, 39.4, 27.9, 27.8, 24.9, 18.8, –1.3. FTIR (thin film) cm^{-1} : 2949 (w), 1669 (s), 1489 (w), 1423 (m), 1249 (m), 1106 (w), 835 (m), 747 (m). HRMS (ESI-FTICR) m/z : $[\text{M} + \text{H}]^+$ calcd for $\text{C}_{22}\text{H}_{33}\text{BrN}_5\text{O}_3\text{Si}$ 556.1585, found 556.1567. TLC (10% methanol in dichloromethane), R_f : 0.59 (UV, CAM).

3-Methylene Azide Derivative 7e. Compound **7e** was synthesized according to the general procedure for synthesis of AgE derivatives using 3-azidopropan-1-ol¹⁵ (415 mg, 4.10 mmol, 20.0 equiv) in dichloromethane (13 mL). The reaction mixture became homogeneous upon addition of methanesulfonic acid. After 14 h, the reaction mixture was diluted with dichloromethane and quenched with aqueous sodium hydroxide solution (0.5 N, 20 mL) before the general workup procedure using dichloromethane. The crude residue was purified by flash column chromatography on silica gel (eluent: 20% acetone in dichloromethane, then 5% → 10% methanol in dichloromethane) to afford 3-methylene azide **7e** (64.4 mg, 74%) as a white solid. ^1H NMR (500 MHz, $\text{DMSO}-d_6$, 23 °C): δ 7.96 (s, 1H), 7.34 (d, $J = 2.1$ Hz, 1H), 6.74 (d, $J = 4.0$ Hz, 1H), 6.35 (d, $J = 4.0$ Hz, 1H), 4.41 (dt, $J = 12.0, 5.9$ Hz, 1H), 4.02 (d, $J = 5.4$ Hz, 1H), 3.97 (d, $J = 1.8$ Hz, 1H), 3.41 (td, $J = 6.6, 2.6$ Hz, 2H), 3.28 (dt, $J = 9.3, 6.2$ Hz, 1H), 3.24–3.17 (m, 1H), 2.65 (s, 3H), 2.56–2.51 (m, 1H), 1.99 (t, $J = 12.6$ Hz, 1H), 1.79 (p, $J = 6.5$ Hz, 2H). ^{13}C NMR (125 MHz, $\text{DMSO}-d_6$, 23 °C): δ 158.7, 157.6, 123.6, 113.5, 112.0, 104.7, 97.5, 60.1, 59.5, 59.3, 51.9, 47.8, 37.7, 28.3, 23.9. FTIR (thin film) cm^{-1} : 2928 (w), 2097 (w), 1666 (s), 1549 (w), 1423 (m), 1348 (w), 1107 (w), 746 (m). HRMS (DART-FTICR) m/z : $[\text{M} + \text{H}]^+$ calcd for $\text{C}_{15}\text{H}_{21}\text{BrN}_5\text{O}_3$ 424.0727, found 424.0717. TLC (10% methanol in dichloromethane), R_f : 0.53 (UV, CAM).

4-Methylene Azide Derivative 7f. Compound **7f** was synthesized according to the general procedure for synthesis of AgE derivatives using 4-azidobutan-1-ol¹⁵ (276 mg, 2.40 mmol, 20.0 equiv) in dichloromethane (8.0 mL). The reaction mixture became homogeneous upon addition of methanesulfonic acid. After 26 h, the reaction mixture was diluted with dichloromethane and quenched with aqueous sodium hydroxide solution (0.5 N, 20 mL) before general workup procedure using dichloromethane. The crude residue was purified by flash column chromatography on silica gel (eluent: 20% acetone in dichloromethane, then 5% → 10% methanol in dichloromethane) to afford 4-methylene azide **7f** (39.8 mg, 76%) as a white solid. ^1H NMR (500 MHz, $\text{DMSO}-d_6$, 23 °C): δ 7.97 (s, 1H), 7.31 (d, $J = 2.0$ Hz, 1H), 6.74 (d, $J = 3.9$ Hz, 1H), 6.35 (d, $J = 4.0$ Hz, 1H), 4.41 (dt, $J = 11.9, 6.0$ Hz, 1H), 4.01 (d, $J = 5.4$ Hz, 1H), 3.97 (d, $J = 2.2$ Hz, 1H), 3.37–3.34 (m, 2H), 3.28–3.19 (m, 1H), 3.19–3.11 (m, 1H), 2.64 (s, 3H), 2.58–2.51 (m, 1H), 1.98 (t, $J = 12.5$ Hz, 1H), 1.64–1.54 (m, 4H). ^{13}C NMR (125 MHz, $\text{DMSO}-d_6$, 23 °C): δ 158.7, 157.6, 123.6, 113.5, 112.0, 104.7, 97.5, 61.6, 60.1, 59.4, 51.9, 50.5, 37.8, 26.3, 25.4,

24.0. FTIR (thin film) cm^{-1} : 2925 (w), 2097 (w), 1668 (s), 1549 (w), 1424 (m), 1107 (w), 745 (w). HRMS (DART-FTICR) m/z : $[\text{M} + \text{H}]^+$ calcd for $\text{C}_{16}\text{H}_{21}\text{BrN}_5\text{O}_3$ 438.0884, found 438.0875. TLC (18% methanol, 2% ammonium hydroxide in chloroform), R_f : 0.43 (UV, CAM).

General Procedure for Staudinger Reduction. Triphenylphosphine (2.40 equiv) was added to a suspension of azide derivative (1 equiv) in tetrahydrofuran–water (9:1, 0.1 M). Upon consumption of starting material as shown by thin-layer chromatography, the reaction mixture was diluted with dichloromethane and concentrated under reduced pressure. The crude residue was purified by flash column chromatography on silica gel (eluent: 0 → 10% methanol in dichloromethane, then 18% methanol and 2% ammonium hydroxide in chloroform) to afford amines **7g–h**.

3-Methylene Amine Derivative 7g. Compound **7g** was synthesized according to the general procedure for Staudinger reduction of azide derivatives using 3-methylene azide **7e** (26.5 mg, 62.5 μmol , 1 equiv). After 3.5 days, the crude residue was purified by flash column chromatography on silica gel to afford amine **7g** (21.9 mg, 88%) as a white solid. ^1H NMR (400 MHz, CD_3OD , 23 °C): δ 6.91 (d, $J = 4.1$ Hz, 1H), 6.33 (d, $J = 4.1$ Hz, 1H), 4.62 (dt, $J = 12.0, 6.0$ Hz, 1H), 4.12 (d, $J = 5.5$ Hz, 1H), 4.09 (s, 1H), 3.50–3.37 (m, 1H), 3.34–3.31 (m, 1H), 2.79 (s, 3H), 2.74 (t, $J = 7.0$ Hz, 2H), 2.71–2.63 (m, 1H), 2.16 (t, $J = 12.7$ Hz, 1H), 1.76 (p, $J = 6.5$ Hz, 2H). ^{13}C NMR (100 MHz, CD_3OD , 23 °C): δ 161.9, 161.1, 124.2, 116.2, 114.0, 107.5, 99.9, 62.2 (2C), 61.7, 53.8, 39.9, 39.4, 33.3, 24.9. FTIR (thin film) cm^{-1} : 2925 (w), 2359 (w), 1695 (m), 1652 (s), 1550 (m), 1424 (m), 1096 (w), 745 (w). HRMS (DART-FTICR) m/z : $[\text{M} + \text{H}]^+$ calcd for $\text{C}_{15}\text{H}_{21}\text{BrN}_5\text{O}_3$ 398.0822, found 398.0823. TLC (18% methanol, 2% ammonium hydroxide in chloroform), R_f : 0.07 (UV, CAM, ninhydrin).

4-Methylene Amine Derivative 7h. Compound **7h** was synthesized according to the general procedure for Staudinger reduction of azide derivatives using 4-methylene azide **7f** (29.0 mg, 66.2 μmol , 1 equiv). After 3 days, the crude residue was purified by flash column chromatography on silica gel to afford 4-methylene amine **7h** (26.6 mg, 97%) as a white solid. ^1H NMR (500 MHz, CD_3OD , 23 °C): δ 6.91 (d, $J = 4.1$ Hz, 1H), 6.33 (d, $J = 3.9$ Hz, 1H), 4.61 (dt, $J = 12.1, 6.0$ Hz, 1H), 4.12 (d, $J = 5.4$ Hz, 1H), 4.08 (s, 1H), 3.38 (dt, $J = 9.1, 5.9$ Hz, 1H), 3.26 (dt, $J = 9.1, 6.1$ Hz, 1H), 2.78 (s, 3H), 2.71–2.63 (m, 3H), 2.15 (t, $J = 12.7$ Hz, 1H), 1.69–1.50 (m, 4H). ^{13}C NMR (125 MHz, CD_3OD , 23 °C): δ 161.8, 161.1, 124.2, 116.2, 114.0, 107.5, 99.8, 63.9, 62.2, 61.7, 53.8, 42.3, 39.4, 30.3, 28.1, 24.9. FTIR (thin film) cm^{-1} : 2926 (w), 2359 (w), 1652 (s), 1550 (m), 1423 (s), 1303 (w), 1096 (m), 745 (m). HRMS (ESI-FTICR) m/z : $[\text{M} + \text{H}]^+$ calcd for $\text{C}_{16}\text{H}_{23}\text{BrN}_5\text{O}_3$ 412.0979, found 412.0994. TLC (18% methanol, 2% ammonium hydroxide in chloroform), R_f : 0.08 (UV, CAM, ninhydrin).

3-Methylene Carbamate Derivative 7i. A solution of 4-nitrophenyl 2-(trimethylsilyl)ethyl carbonate²¹ (5.8 mg, 21 μmol , 1.2 equiv) in dichloromethane (20 μL) was added to a solution of 3-methylene amine **7g** (6.8 mg, 17 μmol , 1 equiv), triethylamine (3.6 μL , 26 μmol , 1.5 equiv), and 4-dimethylaminopyridine (0.4 mg, 3 μmol , 0.2 equiv) in dichloromethane (170 μL). After 26 h, the reaction mixture was diluted with dichloromethane (1 mL) and purified by flash column chromatography on silica gel (eluent: 20% acetone in dichloromethane, then 0 → 18% methanol and 2% ammonium hydroxide in chloroform) to afford 3-methylene carbamate **7i** (8.7 mg, 94%) as a white solid. ^1H NMR (500 MHz, CD_3OD , 23 °C): δ 6.92 (d, $J = 4.2$ Hz, 1H), 6.34 (d, $J = 3.9$ Hz, 1H), 4.61 (dt, $J = 12.1, 6.0$ Hz, 1H), 4.15–4.10 (m, 3H), 4.08 (s, 1H), 3.43–3.34 (m, 1H), 3.30–3.11 (m, 3H), 2.78 (s, 3H), 2.71–2.63 (m, 1H), 2.17 (t, $J = 12.7$ Hz, 1H), 1.77 (p, $J = 6.3$ Hz, 2H), 1.03–0.93 (m, 2H), 0.05 (s, 9H). ^{13}C NMR (125 MHz, CD_3OD , 23 °C): δ 161.8, 161.1, 159.5, 124.2, 116.2, 114.0, 107.5, 99.9, 64.0, 62.2, 61.6 (2C), 53.8, 39.4, 39.0, 31.0, 24.9, 18.8, –1.3. FTIR (thin film) cm^{-1} : 2950 (w), 1698 (s), 1661 (s), 1552 (w), 1424 (m), 1250 (w), 838 (w). HRMS (DART-FTICR) m/z : $[\text{M} + \text{H}]^+$ calcd for $\text{C}_{21}\text{H}_{33}\text{BrN}_5\text{O}_5\text{Si}$ 542.1429, found 542.1429. TLC (18% methanol, 2% ammonium hydroxide in chloroform), R_f : 0.63 (UV, CAM).

General Procedure for Acylation of Amines. Acylating reagent (2.0 equiv) was added to a solution of amine derivative (1 equiv) and

triethylamine (2.0 equiv) in tetrahydrofuran (400 μ L). Upon complete conversion of starting material as shown by thin-layer chromatography, the reaction mixture was diluted with dichloromethane (3 mL) and quenched with saturated aqueous sodium bicarbonate solution (3 mL). Layers were separated, and the aqueous layer was extracted with dichloromethane (3 \times 5 mL). The combined organic layers were dried over anhydrous sodium sulfate, filtered, and concentrated under reduced pressure. The crude residue was purified by flash column chromatography on silica gel (eluent: 0 \rightarrow 7% methanol in dichloromethane, then 9% methanol and 1% ammonium hydroxide in chloroform \rightarrow 18% methanol and 2% ammonium hydroxide in chloroform) to afford amides 7j–k.

Acetamide Derivative 7j. Compound 7j was synthesized according to the general procedure for acylation of amine derivatives using acetic anhydride and amine 7h (6.8 mg, 17 μ mol, 1 equiv) with 4-dimethylaminopyridine (0.4 mg, 3 μ mol, 0.2 equiv) additive. After 2.5 h, the crude residue after workup was purified by flash column chromatography on silica gel to afford acetamide 7j (5.5 mg, 73%) as a white solid. $^1\text{H NMR}$ (500 MHz, CD_3OD , 23 $^\circ\text{C}$): δ 6.91 (d, J = 4.1 Hz, 1H), 6.33 (d, J = 4.0 Hz, 1H), 4.61 (dt, J = 12.1, 6.1 Hz, 1H), 4.12 (d, J = 5.5 Hz, 1H), 4.10 (s, 1H), 3.42–3.36 (m, 1H), 3.29–3.12 (m, 3H), 2.79 (s, 3H), 2.70–2.63 (m, 1H), 2.15 (t, J = 12.7 Hz, 1H), 1.93 (s, 3H), 1.66–1.53 (m, 4H). $^{13}\text{C NMR}$ (125 MHz, CD_3OD , 23 $^\circ\text{C}$): δ 173.4, 161.9, 161.1, 124.2, 116.2, 114.0, 107.5, 99.9, 63.7, 62.2, 61.7, 53.8, 40.2, 39.4, 27.9, 27.4, 24.9, 22.7. FTIR (thin film) cm^{-1} : 2929 (w), 2359 (w), 1652 (s), 1550 (m), 1423 (m), 1373 (w), 1096 (w), 747 (w). HRMS (ESI-FTICR) m/z : $[\text{M} + \text{H}]^+$ calcd for $\text{C}_{18}\text{H}_{25}\text{BrN}_5\text{O}_4$ 454.1084, found 454.1082. TLC (18% methanol, 2% ammonium hydroxide in chloroform), R_f : 0.34 (UV, CAM).

Benzamide Derivative 7k. Compound 7k was synthesized according to the general procedure for acylation of amine derivatives using benzoyl chloride and amine 7h (7.1 mg, 17 μ mol, 1 equiv). After 3.5 h, the crude residue after workup was purified by flash column chromatography on silica gel to afford benzamide 7k (7.7 mg, 87%) as a white solid. $^1\text{H NMR}$ (500 MHz, CD_3OD , 23 $^\circ\text{C}$): δ 7.85–7.78 (m, 2H), 7.56–7.49 (m, 1H), 7.48–7.40 (m, 2H), 6.91 (d, J = 4.1 Hz, 1H), 6.33 (d, J = 3.9 Hz, 1H), 4.61 (dt, J = 12.0, 6.0 Hz, 1H), 4.14 (s, 1H), 4.12 (d, J = 5.4 Hz, 1H), 3.47–3.32 (m, 4H), 2.79 (s, 3H), 2.70–2.63 (m, 1H), 2.16 (t, J = 12.7 Hz, 1H), 1.77–1.65 (m, 4H). $^{13}\text{C NMR}$ (125 MHz, CD_3OD , 23 $^\circ\text{C}$): δ 170.5, 161.9, 161.1, 135.9, 132.7, 129.7, 128.4, 124.2, 116.2, 114.0, 107.5, 99.9, 63.7, 62.3, 61.7, 53.8, 40.8, 39.4, 28.0, 27.5, 24.9. FTIR (thin film) cm^{-1} : 2933 (w), 2359 (w), 1700 (s), 1652 (s), 1550 (m), 1424 (m), 1096 (w), 712 (w). HRMS (ESI-FTICR) m/z : $[\text{M} + \text{H}]^+$ calcd for $\text{C}_{23}\text{H}_{27}\text{BrN}_5\text{O}_4$ 516.1241, found 516.1225. TLC (18% methanol, 2% ammonium hydroxide in chloroform), R_f : 0.50 (UV, CAM).

Urea Intermediate 16. 1,1'-Carbonyldiimidazole (362 mg, 2.23 mmol, 1.10 equiv) and 4-dimethylaminopyridine (37.3 mg, 305 μ mol, 0.150 equiv) were added sequentially to a solution of 1-(tricyclohexylstannyl)-methanamine (15, 808 mg, 2.03 mmol, 1 equiv)²² in dichloromethane (34 mL). After 45 min, the reaction mixture was concentrated, and the crude residue was purified by flash column chromatography on silica gel (eluent: 30 \rightarrow 75% ethyl acetate in hexanes) to afford urea intermediate 16 (847 mg, 85% over two steps) as a white crystalline solid. $^1\text{H NMR}$ (600 MHz, CDCl_3 , 23 $^\circ\text{C}$): δ 8.07 (s, 1H), 7.31 (s, 1H), 7.07 (s, 1H), 6.32 (t, J = 5.5 Hz, 1H), 3.14–3.09 (m, 2H), 1.95–1.81 (m, 6H), 1.72–1.50 (m, 18H), 1.37–1.19 (m, 9H). $^{13}\text{C NMR}$ (100 MHz, CDCl_3 , 23 $^\circ\text{C}$): δ 149.2, 135.7, 129.9, 116.3, 32.4, 29.3, 27.6, 27.2, 23.7. FTIR (thin film) cm^{-1} : 3223 (w), 3036 (w), 2913 (s), 2843 (m), 1710 (s), 1288 (m), 1075 (m), 842 (m). HRMS (ESI-FTICR) m/z : $[\text{M} + \text{H}]^+$ calcd for $\text{C}_{23}\text{H}_{40}\text{N}_3\text{OSn}$ 494.2188, found 494.2223. TLC (50% ethyl acetate in hexanes), R_f : 0.27 (UV, CAM).

General Procedure for the Synthesis of Substituted Ureas. Amine (1.00 equiv) and 4-dimethylaminopyridine (0.150 equiv) were added to a solution of urea intermediate 16 (1 equiv) in dichloromethane (0.2 M). The reaction flask was sealed with a Teflon-wrapped glass stopper and heated to 40 $^\circ\text{C}$. Upon consumption of the starting material as shown by thin-layer chromatography, the reaction mixture was cooled to 23 $^\circ\text{C}$ and

concentrated under reduced pressure. The crude residue was purified by flash column chromatography on silica gel to afford substituted ureas 13a–c.

4-Methylene Alcohol Urea 13a. Compound 13a was prepared according to the general procedure for synthesis of substituted ureas using 4-aminobutanol (156 μ L, 1.69 mmol, 1.00 equiv). After 24 h, the crude residue was purified by flash column chromatography on silica gel (eluent: 30 \rightarrow 100% ethyl acetate in hexanes) to afford 4-methylene alcohol urea 13a (790 mg, 91%) as a white solid. $^1\text{H NMR}$ (600 MHz, CDCl_3 , 23 $^\circ\text{C}$): δ 4.66 (s, 1H), 4.23 (t, J = 4.8 Hz, 1H), 3.69 (q, J = 5.6 Hz, 2H), 3.26 (q, J = 6.3 Hz, 2H), 2.77–2.68 (m, 2H), 1.94–1.77 (m, 6H), 1.72–1.46 (m, 20H), 1.38–1.21 (m, 9H). $^{13}\text{C NMR}$ (125 MHz, CDCl_3 , 23 $^\circ\text{C}$): δ 160.2, 61.9, 40.1, 32.2, 29.7, 29.2, 27.1, 27.0, 26.7, 21.9. FTIR (thin film) cm^{-1} : 3307 (m), 2911 (s), 2841 (m), 1616 (m), 1569 (s), 1443 (m), 990 (m). HRMS (ESI-FTICR) m/z : $[\text{M} + \text{Na}]^+$ calcd for $\text{C}_{24}\text{H}_{46}\text{N}_2\text{NaO}_2\text{Sn}$ 537.2473, found 537.2488. TLC (75% ethyl acetate in hexanes), R_f : 0.28 (UV, CAM).

6-Methylene Alcohol Urea 13b. Compound 13b was prepared according to the general procedure for synthesis of substituted ureas using 6-aminohexanol (357 mg, 3.05 mmol, 1.00 equiv). After 25 h, the crude residue was purified by flash column chromatography on silica gel (eluent: 40 \rightarrow 80% ethyl acetate in hexanes) to afford 6-methylene alcohol urea 13b (1.56 g, 95%) as a white solid. $^1\text{H NMR}$ (500 MHz, CDCl_3 , 23 $^\circ\text{C}$): δ 4.97 (t, J = 5.7 Hz, 1H), 4.62 (s, 1H), 3.56 (q, J = 6.1 Hz, 2H), 3.12 (q, J = 6.7 Hz, 2H), 2.96 (d, J = 5.1 Hz, 1H), 2.78–2.68 (m, 2H), 1.88–1.75 (m, 6H), 1.66–1.44 (m, 22H), 1.38–1.16 (m, 13H). $^{13}\text{C NMR}$ (125 MHz, CDCl_3 , 23 $^\circ\text{C}$): δ 160.0, 62.6, 40.5, 32.7, 32.4, 30.5, 29.3, 27.2, 26.9, 26.6, 25.4, 22.2. FTIR (thin film) cm^{-1} : 3336 (w), 2915 (s), 2845 (s), 1729 (w), 1585 (m), 1444 (m), 991 (m). HRMS (DART-FTICR) m/z : $[\text{M} + \text{H}]^+$ calcd for $\text{C}_{26}\text{H}_{51}\text{N}_2\text{O}_2\text{Sn}$ 543.2967, found 543.2966. TLC (75% ethyl acetate in hexanes), R_f : 0.57 (UV, CAM).

Triethylene Glycol Urea 13c. Compound 13c was prepared according to the general procedure for synthesis of substituted ureas using 2-(2-(2-aminoethoxy)ethoxy)ethanol-1-ol²³ (455 mg, 3.05 mmol, 1.00 equiv). After 24 h, the crude residue was purified by flash column chromatography on silica gel (eluent: 40 \rightarrow 100% ethyl acetate in hexanes) to afford triethylene glycol urea 13c (1.47 g, 84%) as a white solid. $^1\text{H NMR}$ (400 MHz, CDCl_3 , 23 $^\circ\text{C}$): δ 5.13 (t, J = 4.9 Hz, 1H), 4.47 (s, 1H), 3.81–3.75 (m, 2H), 3.73–3.59 (m, 8H), 3.43 (q, J = 5.3 Hz, 2H), 2.88–2.77 (m, 2H), 2.72 (t, J = 6.1 Hz, 1H), 1.96–1.81 (m, 6H), 1.73–1.54 (m, 18H), 1.42–1.21 (m, 9H). $^{13}\text{C NMR}$ (125 MHz, CDCl_3 , 23 $^\circ\text{C}$): δ 159.9, 72.6, 70.9, 70.5 (2C), 61.9, 40.5, 32.4, 29.3, 27.2, 26.9, 22.2. FTIR (thin film) cm^{-1} : 3339 (w), 2914 (s), 2845 (s), 1729 (w), 1553 (m), 1445 (m), 1070 (s), 991 (m). HRMS (ESI-FTICR) m/z : $[\text{M} + \text{Na}]^+$ calcd for $\text{C}_{26}\text{H}_{50}\text{N}_2\text{NaO}_4\text{Sn}$ 597.2685, found 597.2714. TLC (75% ethyl acetate in hexanes), R_f : 0.18 (UV, CAM).

4-Methylene Alcohol Preagelastatin 11a. Compound 11a was prepared according to our published procedure for synthesis of preagelastatins^{3a} using urea 13a (659 mg, 1.28 mmol, 3.00 equiv). The crude residue adsorbed onto silica gel was purified by flash column chromatography on silica gel (eluent: 9% methanol and 1% ammonium hydroxide in chloroform \rightarrow 18% methanol and 2% ammonium hydroxide in chloroform) to afford 4-methylene alcohol preagelastatin 11a (94 mg, 53% over two steps) as an off-white solid. $^1\text{H NMR}$ (600 MHz, CD_3OD , 23 $^\circ\text{C}$): δ 6.91 (d, J = 4.0 Hz, 1H), 6.28 (d, J = 4.0 Hz, 1H), 6.00 (s, 1H), 4.78–4.75 (m, 1H), 4.58–4.52 (m, 1H), 3.68–3.60 (m, 1H), 3.58–3.55 (m, 2H), 3.52–3.46 (m, 1H), 3.34 (s, 3H), 2.93 (dd, J = 15.5, 6.8 Hz, 1H), 2.78 (dd, J = 15.5, 7.9 Hz, 1H), 1.71–1.64 (m, 2H), 1.54–1.51 (m, 2H). $^{13}\text{C NMR}$ (125 MHz, CD_3OD , 23 $^\circ\text{C}$): δ 161.1, 155.9, 124.5, 119.7, 116.1, 113.5, 108.8, 108.7, 84.7, 62.5, 58.2, 55.2, 41.9, 30.8, 29.5, 27.5. FTIR (thin film) cm^{-1} : 3207 (br-m), 2932 (w), 2871 (w), 1652 (s), 1550 (m), 1418 (m), 1076 (s). HRMS (DART-FTICR) m/z : $[\text{M} + \text{H}]^+$ calcd for $\text{C}_{16}\text{H}_{22}\text{BrN}_4\text{O}_4$ 413.0819, found 413.0816. TLC (18% methanol, 2% ammonium hydroxide in chloroform), R_f : 0.31 (UV, CAM).

6-Methylene Alcohol Preagelastatin 11b. Compound 11b was prepared according to our published procedure for synthesis of preagelastatins^{3a} using urea 13b (975 mg, 1.80 mmol, 3.00 equiv). The crude residue adsorbed onto silica gel was purified by flash column

chromatography on silica gel (eluent: 6% methanol and 0.6% ammonium hydroxide in chloroform → 14% methanol and 1.6% ammonium hydroxide in chloroform) to afford 6-methylene alcohol preagelastatin **11b** (178 mg, 67% over two steps) as an off-white solid. ¹H NMR (500 MHz, CD₃OD, 23 °C): δ 6.91 (d, *J* = 4.1 Hz, 1H), 6.28 (d, *J* = 4.1 Hz, 1H), 6.02 (s, 1H), 4.76 (d, *J* = 1.4 Hz, 1H), 4.58–4.52 (m, 1H), 3.63–3.51 (m, 3H), 3.44–3.38 (m, 1H), 3.34 (s, 3H), 2.92 (dd, *J* = 15.4, 6.7 Hz, 1H), 2.77 (ddd, *J* = 15.4, 7.9, 0.9 Hz, 1H), 1.65–1.49 (m, 4H), 1.42–1.30 (m, 4H). ¹³C NMR (125 MHz, CD₃OD, 23 °C): δ 161.1, 155.9, 124.5, 119.8, 116.1, 113.6, 108.7 (2C), 84.7, 62.9, 58.3, 55.2, 42.0, 33.6, 30.9, 29.6, 27.7, 26.7. FTIR (thin film) cm⁻¹: 3212 (br-m), 2931 (m), 2857 (w), 1658 (s), 1551 (w), 1419 (m), 1084 (m). HRMS (DART-FTICR) *m/z*: [M + H]⁺ calcd for C₁₈H₂₆BrN₄O₄ 441.1132, found 441.1132. TLC (18% methanol, 2% ammonium hydroxide in chloroform), *R*_f: 0.56 (UV, CAM).

Triethylene Glycol Preagelastatin 11c. Compound **11c** was prepared according to our published procedure for synthesis of preagelastatins^{3a} using urea **13c** (1.29 g, 2.25 mmol, 3.00 equiv). The crude residue adsorbed onto silica gel was purified by flash column chromatography on silica gel (eluent: 9% methanol and 1% ammonium hydroxide in chloroform → 18% methanol and 2% ammonium hydroxide in chloroform) to afford triethylene glycol preagelastatin **11c** (218 mg, 61% over two steps) as an off-white solid. ¹H NMR (400 MHz, CD₃OD, 23 °C): δ 6.91 (d, *J* = 4.1 Hz, 1H), 6.27 (d, *J* = 4.0 Hz, 1H), 5.97 (s, 1H), 4.76 (d, *J* = 1.5 Hz, 1H), 4.69 (td, *J* = 7.4, 1.5 Hz, 1H), 3.70–3.65 (m, 2H), 3.65–3.61 (m, 4H), 3.60–3.55 (m, 4H), 3.54–3.47 (m, 2H), 3.34 (s, 3H), 2.99 (dd, *J* = 15.5, 6.9 Hz, 1H), 2.83 (dd, *J* = 15.5, 7.8 Hz, 1H). ¹³C NMR (100 MHz, CD₃OD, 23 °C): δ 161.2, 155.9, 124.5, 120.9, 116.0, 113.4, 108.8, 108.2, 84.7, 73.8, 71.8, 71.5, 70.6, 62.3, 57.9, 55.2, 42.7, 29.7. FTIR (thin film) cm⁻¹: 3226 (br-m), 2921 (m), 2870 (m), 1652 (s), 1419 (m), 1086 (m). HRMS (DART-FTICR) *m/z*: [M + H]⁺ calcd for C₁₈H₂₆BrN₄O₆ 473.1030, found 473.1021. TLC (18% methanol, 2% ammonium hydroxide in chloroform), *R*_f: 0.47 (UV, CAM).

4-Methylene Alcohol Derivative 8a and Pentacyclic Derivative 14. Compounds **8a** and **14** were prepared according to our published procedure for synthesis of (–)-agelastatin A^{3a} using 4-methylene alcohol preagelastatin **11a** (26.0 mg, 63.0 μmol, 1 equiv). The crude residue adsorbed onto silica gel was purified by flash column chromatography on silica gel (chloroform → 18% methanol and 2% ammonium hydroxide in chloroform) to afford 4-methylene alcohol derivative **8a** (0.8 mg, 3%) as an off-white solid along with the pentacyclic derivative **14** (2.6 mg, 11%) as an off-white solid. **4-Methylene Alcohol Derivative 8a.** ¹H NMR (600 MHz, CD₃OD, 23 °C): δ 6.91 (d, *J* = 4.1 Hz, 1H), 6.33 (d, *J* = 4.1 Hz, 1H), 4.65 (dt, *J* = 12.0, 5.9 Hz, 1H), 4.09 (d, *J* = 5.5 Hz, 1H), 3.86 (s, 1H), 3.61 (td, *J* = 6.6, 2.8 Hz, 2H), 3.30–3.18 (m, 2H), 2.65 (dd, *J* = 13.1, 6.3 Hz, 1H), 2.17 (t, *J* = 12.7 Hz, 1H), 1.84–1.75 (m, 2H), 1.62 (p, *J* = 6.8 Hz, 2H). ¹³C NMR (100 MHz, CD₃OD, 23 °C): δ 161.9, 161.2, 124.3, 116.2, 113.9, 107.4, 96.1, 67.7, 62.8, 62.4, 54.5, 41.3, 40.3, 31.4, 28.0. FTIR (thin film) cm⁻¹: 3276 (br-s), 2933 (w), 1653 (s), 1552 (w), 1424 (m), 1375 (w). HRMS (DART-FTICR) *m/z*: [M + H]⁺ calcd for C₁₅H₂₀BrN₄O₄ 399.0662, found 399.0655. TLC (18% methanol, 2% ammonium hydroxide in chloroform), *R*_f: 0.19 (UV, CAM). **Pentacyclic Derivative 14.** ¹H NMR (500 MHz, CD₃OD, 23 °C): δ 6.91 (d, *J* = 4.1 Hz, 1H), 6.33 (d, *J* = 4.1 Hz, 1H), 4.64 (dt, *J* = 12.0, 6.0 Hz, 1H), 4.14 (d, *J* = 5.3 Hz, 1H), 3.95 (s, 1H), 3.87 (d, *J* = 12.9 Hz, 1H), 3.79 (d, *J* = 14.4 Hz, 1H), 3.41–3.32 (m, 2H), 2.97–2.89 (m, 1H), 2.50 (dd, *J* = 13.1, 6.7 Hz, 1H), 2.14 (t, *J* = 12.6 Hz, 1H), 1.77–1.59 (m, 4H). ¹³C NMR (100 MHz, CD₃OD, 23 °C): δ 161.9, 161.2, 124.3, 116.3, 114.0, 107.5, 100.7, 66.2, 64.8, 62.0, 54.2, 41.9, 41.2, 31.3, 27.4. FTIR (thin film) cm⁻¹: 3247 (br-m), 2940 (m), 1696 (s), 1659 (s), 1552 (m), 1422 (s), 1091 (m). HRMS (DART-FTICR) *m/z*: [M + H]⁺ calcd for C₁₅H₁₈BrN₄O₃ 381.0557, found 381.0552. TLC (18% methanol, 2% ammonium hydroxide in chloroform), *R*_f: 0.59 (UV, CAM).

6-Methylene Alcohol Derivative 8b. Compound **8b** was prepared according to our published procedure for synthesis of (–)-agelastatin A^{3a} using 6-methylene alcohol preagelastatin **11b** (1.00 × 10² mg, 227 μmol, 1 equiv). The crude residue adsorbed onto silica

gel was purified by flash column chromatography on silica gel (6% methanol and 0.6% ammonium hydroxide in chloroform → 18% methanol and 2% ammonium hydroxide in chloroform) to afford 6-methylene alcohol derivative **8b** (35 mg, 36%) as an off-white solid. ¹H NMR (400 MHz, CD₃OD, 23 °C): δ 6.91 (d, *J* = 4.0 Hz, 1H), 6.33 (d, *J* = 4.1 Hz, 1H), 4.63 (dt, *J* = 12.0, 5.9 Hz, 1H), 4.09 (d, *J* = 5.5 Hz, 1H), 3.85 (s, 1H), 3.56 (t, *J* = 6.5 Hz, 2H), 3.28–3.15 (m, 2H), 2.63 (dd, *J* = 13.0, 6.3 Hz, 1H), 2.17 (t, *J* = 12.6 Hz, 1H), 1.84–1.67 (m, 2H), 1.62–1.52 (m, 2H), 1.47–1.39 (m, 4H). ¹³C NMR (100 MHz, CD₃OD, 23 °C): δ 161.9, 161.2, 124.3, 116.2, 114.0, 107.3, 96.1, 67.7, 63.0, 62.4, 54.5, 41.4, 40.4, 33.8, 31.5, 28.3, 26.9. FTIR (thin film) cm⁻¹: 3254 (br-s), 2929 (m), 2856 (m), 1652 (s), 1551 (m), 1422 (s), 1027 (w). HRMS (DART-FTICR) *m/z*: [M + H]⁺ calcd for C₁₇H₂₄BrN₄O₄ 427.0975, found 427.0970. TLC (18% methanol, 2% ammonium hydroxide in chloroform), *R*_f: 0.27 (UV, CAM).

Triethylene Glycol Derivative 8c. Compound **8c** was prepared according to our published procedure for synthesis of (–)-agelastatin A^{3a} using triethylene glycol preagelastatin **11c** (1.80 × 10² mg, 3.80 × 10² μmol, 1 equiv). The crude residue adsorbed onto silica gel was purified by flash column chromatography on silica gel (6% methanol and 0.6% ammonium hydroxide in chloroform → 18% methanol and 2% ammonium hydroxide in chloroform) to afford triethylene glycol derivative **8c** (52 mg, 30%) as an off-white solid. ¹H NMR (600 MHz, CD₃OD, 23 °C): δ 6.92 (d, *J* = 3.9 Hz, 1H), 6.33 (d, *J* = 3.9 Hz, 1H), 4.64 (dt, *J* = 12.1, 6.0 Hz, 1H), 4.09 (d, *J* = 5.7 Hz, 1H), 3.89 (s, 1H), 3.73–3.62 (m, 9H), 3.59–3.48 (m, 2H), 3.42–3.33 (m, 1H), 2.79 (dd, *J* = 12.9, 6.4 Hz, 1H), 2.13 (t, *J* = 12.6 Hz, 1H). ¹³C NMR (125 MHz, CD₃OD, 23 °C): δ 161.7, 161.2, 124.3, 116.2, 113.9, 107.4, 95.9, 73.8, 71.6, 71.5, 70.6, 67.8, 62.3, 62.2, 54.6, 41.5, 40.1. FTIR (thin film) cm⁻¹: 3264 (br-s), 2921 (w), 1645 (s), 1551 (m), 1093 (m), 1024 (m). HRMS (DART-FTICR) *m/z*: [M + H]⁺ calcd for C₁₇H₂₄BrN₄O₆ 459.0874, found 459.0895. TLC (18% methanol, 2% ammonium hydroxide in chloroform), *R*_f: 0.35 (UV, CAM).

General Procedure for the Synthesis of Azide Derivatives. Alcohol derivative (1 equiv) and triphenylphosphine were dissolved in tetrahydrofuran. After 5 min, diisopropylazodicarboxylate and diphenylphosphorylazide were added sequentially. After 21 h or upon consumption of starting material as shown by thin-layer chromatography, the reaction mixture was concentrated under reduced pressure. The crude residue was purified by flash column chromatography on silica gel to afford azide derivatives **8d–e**.

6-Methylene Azide Derivative 8d. Compound **8d** was synthesized from 6-methylene alcohol derivative **8b** according to the general procedure for the synthesis of azide derivatives using triphenylphosphine (12.6 mg, 48.0 μmol, 2.00 equiv), diisopropylazodicarboxylate (9.4 μL, 48 μmol, 2.0 equiv), and diphenylphosphorylazide (10.6 μL, 48.0 μmol, 2.00 equiv) in tetrahydrofuran (350 μL). After 21 h, the crude residue was purified by flash column chromatography on silica gel (chloroform → 18% methanol and 2% ammonium hydroxide in chloroform) to afford 6-methylene azide derivative **8d** (4.2 mg, 38%) as a white solid along with recovered 6-methylene alcohol derivative **8b** (3.5 mg, 34%). Reaction yield was 72% based on recovered starting material. ¹H NMR (600 MHz, CD₃OD, 23 °C): δ 6.91 (d, *J* = 4.1 Hz, 1H), 6.34 (d, *J* = 4.1 Hz, 1H), 4.64 (dt, *J* = 12.1, 5.9 Hz, 1H), 4.09 (d, *J* = 5.5 Hz, 1H), 3.86 (s, 1H), 3.31–3.16 (m, 2H), 2.63 (dd, *J* = 13.1, 6.3 Hz, 1H), 2.17 (t, *J* = 12.6 Hz, 1H), 1.83–1.67 (m, 2H), 1.66–1.37 (m, 6H), 1.32–1.22 (m, 2H). ¹³C NMR (125 MHz, CD₃OD, 23 °C): δ 161.9, 161.2, 124.3, 116.2, 114.0, 107.2, 96.1, 67.7, 62.4, 54.5, 52.5, 41.4, 40.3, 31.4, 30.0, 27.9, 27.8. FTIR (thin film) cm⁻¹: 3222 (br-m), 2930 (m), 2856 (s), 2095 (s), 1669 (s), 1118 (m). HRMS (DART-FTICR) *m/z*: [M + H]⁺ calcd for C₁₇H₂₃BrN₇O₃ 452.1040, found 452.1058. TLC (9% methanol, 1% ammonium hydroxide in chloroform), *R*_f: 0.28 (UV, CAM).

Triethylene Glycol Bis-azide Derivative 8e. Compound **8e** was synthesized from triethylene glycol derivative **8c** according to the general procedure for the synthesis of azide derivatives using triphenylphosphine (36.0 mg, 137 μmol, 10.0 equiv), diisopropylazodicarboxylate (27.0 μL, 137 μmol, 10.0 equiv), and diphenylphosphorylazide (31.0 μL, 137 μmol, 10.0 equiv) in tetrahydrofuran (274 μL). After 6 h, the crude residue was purified by flash column

chromatography on silica gel (chloroform \rightarrow 18% methanol and 2% ammonium hydroxide in chloroform) to afford triethylene glycol bis-azide derivative **8e** (3.7 mg, 54%) as a white solid. ^1H NMR (500 MHz, CD_3OD , 23 $^\circ\text{C}$): δ 6.93 (d, J = 4.1 Hz, 1H), 6.35 (d, J = 4.0 Hz, 1H), 4.79 (dt, J = 12.1, 6.2 Hz, 1H), 4.23 (s, 1H), 4.18 (d, J = 5.5 Hz, 1H), 3.82–3.56 (m, 6H), 3.53 (t, J = 5.7 Hz, 2H), 3.35–3.32 (m, 2H), 2.98 (dd, J = 13.5, 6.5 Hz, 1H), 2.13–2.06 (m, 1H), 1.35–1.26 (m, 2H). ^{13}C NMR (125 MHz, CD_3OD , 23 $^\circ\text{C}$): δ 161.3, 161.0, 124.2, 116.4, 114.1, 107.7, 88.5, 71.7 (2C), 71.3, 70.4, 66.1, 62.1, 54.5, 51.9, 41.5, 39.9. FTIR (thin film) cm^{-1} : 3255 (br-w), 2920 (m), 2852 (w), 2105 (s), 1700 (m), 1662 (s), 1424 (m), 1102 (br-m). HRMS (ESI-FTICR) m/z : $[\text{M} + \text{H}]^+$ calcd for $\text{C}_{17}\text{H}_{22}\text{BrN}_{10}\text{O}_4$ 509.1003, found 509.0990. TLC (18% methanol, 2% ammonium hydroxide in chloroform), R_f : 0.50 (UV, CAM).

Cell Culture Methods. All RMF cell lines were grown in Dulbecco's modified Eagle's medium (DMEM) supplemented with 10% bovine calf serum. The human breast cancer cell line, SUM1315, was grown in Ham's F12 nutrient mixture with 5% fetal bovine serum, 10 ng/mL epidermal growth factor (EGF), and 5 $\mu\text{g}/\text{mL}$ insulin. All culture media contained 100 Units/mL penicillin, 100 $\mu\text{g}/\mu\text{L}$ streptomycin, and 0.1% fungizone. The parental RMF cell line expressing green fluorescent protein (GFP) and the human breast cancer cell line SUM1315 were kind gifts from Dr. Charlotte Kuperwasser, Tufts University.²⁴ Derivation of the stable fibroblast sublines shTiam-RMF and C-RMF has been described previously.¹¹

Quantitative Reverse Transcription Polymerase Chain Reaction (RT-PCR) for OPN (Figures 3 and 8). Total RNA synthesis was carried out using the acid guanidinium thiocyanate–phenol–chloroform extraction method²⁵ per manufacturer protocol. First-strand cDNA synthesis was performed using a version of Moloney murine leukemia virus reverse transcriptase per manufacturer protocol. Some mammary fibroblasts were treated with 10 nM vitamin D and AgA, AgE, or agelastatin derivative as indicated for 48 h prior to assay. Quantitative PCR was performed in triplicate reactions in 20 μL volumes containing cDNA with cyanine dye and DNA polymerase master mix using the following primer sets: glyceraldehyde 3-phosphate dehydrogenase (GAPDH), 5'-CTGCACCACCAACTGCTTAG-3' (sense), 5'-TTCAGCTCAGGGATGACCTT-3' (antisense); OPN, 5'-GCCATACCAGTTAAACAGGC-3' (sense), 5'-GACCTCAGAAGATGCACTAT-3' (antisense). Real-time PCR parameters: 95 $^\circ\text{C}$ for 10 min; 95 $^\circ\text{C}$ for 30 s, 60 $^\circ\text{C}$ for 60 s, 72 $^\circ\text{C}$ for 60 s for 40 cycles. Data analysis was done using a continuous fluorescence detector. The comparative threshold cycle ($2^{-\Delta\Delta\text{CT}}$) value²⁶ was calculated following GAPDH normalization. Results indicate mean \pm standard deviation and represent a composite of at least duplicate experiments, each with triplicate conditions.

Spheroid Coculture Methods (Figure 4). Three-dimensional cocultures with SUM1315 cells and fibroblast lines were established in phenol-red free basement membrane matrix from the Engelbreth–Holm–Swarm mouse sarcoma (medium mixture as previously described).⁸ Cultures had equal volumes of DMSO, AgA, or AgE incorporated into the matrix and culture medium at the indicated concentrations. Stock solutions (1 mM) were stored in DMSO at -20 $^\circ\text{C}$, and diluted in culture medium to indicated final concentrations. Number of projections per spheroid was quantified using an Eclipse TS100 inverted tissue culture microscope and depicted as number of spheroids with indicated number of projections as percent of total spheroids. At least 100 spheroids were counted for each experimental condition. Results are representative of duplicate experiments. Cells were isolated from 3D cocultures and cancer cells were separated from fibroblasts as described previously.⁸ Flow cytometry was used to demonstrate purity of cells isolated postcoculture to greater than 99% cancer cells using GFP markers to identify RMFs.

Transwell Migration Assays (Figure 5). Transwell migration of SUM1315 after isolation from mixed cell spheroid cocultures with indicated mammary fibroblasts, with or without indicated agelastatin compound, was used to assess adhesion of PCC cells. Cultured cells were deprived of serum overnight, trypsinized, and plated at a density of $1 \times 10^5/\text{mL}$ (2×10^4 cells/basket) in the upper basket of transwell chambers with a filter pore size of 8 μm . Cells were allowed to migrate

for 5 h at 37 $^\circ\text{C}$ toward lower chambers containing either DMEM alone or supplemented with 25% filter-sterilized conditioned medium harvested from NIH3T3 cells. Nonmigrated cells were then removed from the upper side of the filter using a cotton swab. Filters were fixed and stained with a three-step hematology stain protocol comparable to the Wright–Giemsa method. Filters were cut out and mounted on glass slides under coverslips using microscope immersion oil. Migrated cells were counted in nine random fields for each replicate of biologic triplicates using an Eclipse TS100 microscope and 20 \times objective. Results are representative of duplicate experiments.

Tumorsphere Assays (Figure 6). The SUM1315 breast cancer cells isolated from 3D cocultures with indicated mammary fibroblasts and indicated concentrations of AgA or AgE were trypsinized and cell clumps were broken up by gentle pipetting several times. After low-speed centrifugation (1200 rpm), cell pellets were resuspended in corresponding culture medium, and passed through a 40 μm filter to obtain single cell suspensions. Five thousand cells in 4 mL culture medium were plated per well in ultralow attachment six-well plates. Tumorspheres were quantitated within 10–14 days in culture and sphere images were obtained on an Eclipse TS100 inverted microscope. Results are representative of duplicate experiments, each with biologic triplicates.

Flow Cytometry Assays (Figure 7). Populations of SUM1315 breast cancer cells were quantified by flow cytometry for expression of indicated cell surface markers using fluorophore-conjugated antibodies after isolation from 3D cocultures with indicated fibroblasts. Aliquots of 0.5×10^6 cells in 100 μL of fluorescence-activated cell sorting buffer (phosphate-buffered saline with 2% bovine serum albumin) were stained with epithelial cell adhesion molecule epithelial specific antigen (ESA) fluorescein isothiocyanate (FITC) [clone VU-ID9, 1:10], CD24-phycoerythrin (PE) [clone ML5, 1:400], and CD44-allophycocyanin (APC) [clone G44–26, 1:50] antibodies in the dark at room temperature for 30 min. At the end of incubation, 900 μL of fluorescence-activated cell sorting buffer was added to the cell/antibody mixture, and cells were then analyzed using an advanced digital processing analyzer. To set background gating, other cell aliquots were stained with isotype control antibodies conjugated with corresponding fluorophore [APC mouse immunoglobulin G (IgG) subclass 2b kappa (κ); PE mouse IgG2a κ ; FITC mouse IgG] so that the nonspecific CD44 $^+$ /CD24 $^-$ /ESA $^+$ staining represented less than 0.5% of the cell population. Cells were first gated using APC and PE to identify the CD44 $^+$ /CD24 $^-$ population, followed by secondary gating on FITC to identify the CD44 $^+$ /CD24 $^-$ /ESA $^+$ cells. Results are representative of duplicate experiments, each with biologic triplicates.

Effects of Agelastatin Derivatives (Figure 8). Quantitative RT-PCR for OPN mRNA relative to GAPDH control from mammary fibroblasts treated with vitamin D, and AgA, AgE, or agelastatin derivative as indicated for 48 h. Results indicate mean \pm standard deviation and represent a composite of at least duplicate experiments, each with triplicate conditions. Detailed experimental methods are described above for Figure 3.

■ ASSOCIATED CONTENT

📄 Supporting Information

The Supporting Information is available free of charge on the ACS Publications website at DOI: 10.1021/acs.joc.7b01162.

^1H and ^{13}C NMR spectra of all compounds described in the Experimental Section (PDF)

■ AUTHOR INFORMATION

Corresponding Author

*E-mail: movassag@mit.edu.

ORCID

Mohammad Movassaghi: 0000-0003-3080-1063

Notes

The authors declare no competing financial interest.

ACKNOWLEDGMENTS

M.M. and A.H.A. acknowledge financial support by NIH-NIGMS (GM074825) and Amgen. R.J.B. and K.X. acknowledge financial support by the US Department of Defense (W81XWH-11-1-0814) and the Diane Connolly-Zaniboni Research Scholarship in Breast Cancer at Tufts Medical Center. A.H.A. acknowledges an Amgen Graduate Fellowship in Synthetic Chemistry.

REFERENCES

- (1) (a) D'Ambrosio, M.; Guerriero, A.; Debitus, C.; Ribes, O.; Pusset, J.; Leroy, S.; Pietra, F. *J. Chem. Soc., Chem. Commun.* **1993**, 1305–1306. (b) Guerriero, A.; D'Ambrosio, M.; Chiasera, G.; Pietra, F. *Helv. Chim. Acta* **1994**, *77*, 1895–1902. (c) D'Ambrosio, M.; Guerriero, A.; Ripamonti, M.; Debitus, C.; Waikedre, J.; Pietra, F. *Helv. Chim. Acta* **1996**, *79*, 727–735. (d) Pettit, G. R.; Ducki, S.; Herald, D. L.; Doubek, D. L.; Schmidt, J. M.; Chapuis, J.-C. *Oncol. Res.* **2005**, *15*, 11–20. (e) Hong, T. W.; Jimenez, D. R.; Molinski, T. F. *J. Nat. Prod.* **1998**, *61*, 158–161. (f) Tilvi, S.; Moriou, C.; Martin, M.-T.; Gallard, J.-F.; Sorres, J.; Patel, K.; Petek, S.; Debitus, C.; Ermolenko, L.; Al-Mourabit, A. *J. Nat. Prod.* **2010**, *73*, 720–723.
- (2) (a) Meijer, L.; Thunnissen, A.; White, A. W.; Garnier, M.; Nikolic, M.; Tsai, L.; Walter, J.; Cleverley, K. E.; Salinas, P. C.; Wu, Y.; Biernat, J.; Mandelkow, E.; Kim, S.; Pettit, G. R. *Chem. Biol.* **2000**, *7*, 51–63. (b) Hale, K. J.; Domostoj, M. M.; El-Tanani, M.; Campbell, F. C.; Mason, C. K. In *Strategies and Tactics in Organic Synthesis*; Harmata, M., Ed.; Elsevier Academic Press: London, 2005; Vol. 6, Chapter 11, pp 352–394. (c) Mason, C. K.; McFarlane, S.; Johnston, P. G.; Crowe, P.; Erwin, P. J.; Domostoj, M. M.; Campbell, F. C.; Manaviar, S.; Hale, K. J.; El-Tanani, M. *Mol. Cancer Ther.* **2008**, *7*, 548–558. (d) Li, Z.; Kamon, T.; Personett, D. A.; Caulfield, T.; Copland, J. A.; Yoshimitsu, T.; Tun, H. W. *MedChemComm* **2012**, *3*, 233–237. (e) Li, Z.; Shigeoka, D.; Caulfield, T. R.; Kawachi, T.; Qiu, Y.; Kamon, T.; Arai, M.; Tun, H. W.; Yoshimitsu, T. *MedChemComm* **2013**, *4*, 1093–1098.
- (3) (a) Movassaghi, M.; Siegel, D. S.; Han, S. *Chem. Sci.* **2010**, *1*, 561–566. (b) Han, S.; Siegel, D. S.; Morrison, K. C.; Hergenrother, P. J.; Movassaghi, M. *J. Org. Chem.* **2013**, *78*, 11970. (c) Movassaghi, M.; Hergenrother, P. J. *Compounds, Compositions and Methods of Agelastatin Alkaloids*. U.S. Patent 9,434,736, September 6, 2016.
- (4) For a review on total synthesis of agelastatin alkaloids, see: (a) Dong, G. *Pure Appl. Chem.* **2010**, *82*, 2231–2246. For representative total syntheses of agelastatin alkaloids, see: (b) Stien, D.; Anderson, G. T.; Chase, C. E.; Koh, Y.; Weinreb, S. M. *J. Am. Chem. Soc.* **1999**, *121*, 9574–9579. (c) Feldman, K. S.; Saunders, J. C. *J. Am. Chem. Soc.* **2002**, *124*, 9060–9061. (d) Feldman, K. S.; Saunders, J. C.; Wroblewski, M. L. *J. Org. Chem.* **2002**, *67*, 7096–7109. (e) Davis, F. A.; Deng, J. *Org. Lett.* **2005**, *7*, 621–623. (f) Wehn, P. M.; Du Bois, J. *Angew. Chem., Int. Ed.* **2009**, *48*, 3802–3805. (g) Trost, B. M.; Dong, G. *Chem. - Eur. J.* **2009**, *15*, 6910–6919.
- (5) For representative recent total syntheses of agelastatin alkaloids, see: (a) Reyes, J. C. P.; Romo, D. *Angew. Chem., Int. Ed.* **2012**, *51*, 6870–6873. (b) Duspara, P. A.; Batey, R. A. *Angew. Chem., Int. Ed.* **2013**, *52*, 10862–10866. For recent formal total syntheses of agelastatin alkaloids, see: (c) Menjo, Y.; Hamajima, A.; Sasaki, N.; Hamada, Y. *Org. Lett.* **2011**, *13*, 5744–5747. (d) Kano, T.; Sakamoto, R.; Akakura, M.; Maruoka, K. *J. Am. Chem. Soc.* **2012**, *134*, 7516–7520. (e) Shigeoka, D.; Kamon, T.; Yoshimitsu, T. *Beilstein J. Org. Chem.* **2013**, *9*, 860–865.
- (6) (a) Stout, P. E.; Choi, M. Y.; Castro, J. E.; Molinski, T. F. *J. Med. Chem.* **2014**, *57*, 5085–5093. (b) Jouanneau, M.; McClary, B.; Reyes, J. C. P.; Chen, R.; Chen, Y.; Plunkett, W.; Cheng, X.; Milinichik, A. Z.; Albone, E. F.; Liu, J. O.; Romo, D. *Bioorg. Med. Chem. Lett.* **2016**, *26*, 2092–2097. (c) Tun, H. W.; Yoshimitsu, T.; Shigeoka, D.; Kamon, T.; Li, Z.; Qiu, Y.; Caulfield, T. R. *Substituted Imidazo[4',5':4,5]cyclopenta[1,2-e]pyrrolo[1,2-a]pyrazines and Oxazolo[4',5':4,5]cyclopenta[1,2-e]pyrrolo[1,2-a]pyrazines for Treating Brain Cancer*. U.S. Patent 9,464,093, October 11, 2016. (d) McClary, B.; Zinshteyn, B.; Meyer, M.; Jouanneau, M.; Pellegrino, S.; Yusupova, G.; Schuller, A.; Reyes, J. C. P.; Lu, J.; Guo, Z.; Ayinde, S.; Luo, C.; Dang, Y.; Romo, D.; Yusupov, M.; Green, R.; Liu, J. O. *Cell Chem. Biol.* **2017**, *24*, 605–613.
- (7) Han, S.; Siegel, D. S.; Movassaghi, M. *Tetrahedron Lett.* **2012**, *53*, 3722–3723.
- (8) Xu, K.; Buchsbaum, R. J. *J. Visualized Exp.* **2012**, *62*, e3760.
- (9) Xu, K.; Tian, X.; Oh, S. Y.; Movassaghi, M.; Naber, S. P.; Kuperwasser, C.; Buchsbaum, R. J. *Breast Cancer Res.* **2016**, *18*, 14.
- (10) Liu, J.; Xu, K.; Chase, M.; Ji, Y.; Logan, J. K.; Buchsbaum, R. J. *J. Cell Sci.* **2012**, *125*, 376–386.
- (11) Xu, K.; Rajagopal, S.; Klebba, I.; Dong, S.; Ji, Y.; Liu, J.; Kuperwasser, C.; Garlick, J. A.; Naber, S. P.; Buchsbaum, R. J. *Oncogene* **2010**, *29*, 6533–6542.
- (12) Mice developed hunched posture, decreased mobility, fur ruffling, and lack of weight gain, leading to termination of experiment per established animal protocol guidelines.
- (13) These studies were analogous with those detailed in ref 9 for (–)-agelastatin A.
- (14) Coste, A.; Kim, J.; Adams, T. C.; Movassaghi, M. *Chem. Sci.* **2013**, *4*, 3191–3197.
- (15) Mantovani, G.; Ladmiral, V.; Tao, L.; Haddleton, D. M. *Chem. Commun.* **2005**, 2089–2091.
- (16) For discussion of the use of 1,1'-carbonyldiimidazole in urea synthesis, see: Duspara, P. A.; Islam, Md. S.; Lough, A. J.; Batey, R. A. *J. Org. Chem.* **2012**, *77*, 10362–10368 and references cited therein.
- (17) For a review on synthetic methodologies for substituted ureas, see: Gallou, I. *Org. Prep. Proced. Int.* **2007**, *39*, 355–383.
- (18) In prior assays of the natural agelastatin alkaloids, we have observed that differential activity against stimulated OPN transcription in 2D assays correlates exactly with differential potency in the more complex biologic assays.
- (19) Still, W. C.; Kahn, M.; Mitra, A. *J. Org. Chem.* **1978**, *43*, 2923–2925.
- (20) Kromann, H.; Krikstolaiyte, S.; Andersen, A. J.; Andersen, K.; Krogsgaard-Larsen, P.; Jaroszewski, J. W.; Egebjerg, J.; Strømgaard, K. *J. Med. Chem.* **2002**, *45*, 5745–5754.
- (21) Okoth, R.; Basu, A. *Beilstein J. Org. Chem.* **2013**, *9*, 608–612.
- (22) Synthesized from tricyclohexyltin chloride and diiodomethane according to our protocol described in ref 3a. Due to the high sensitivity of 1-(tricyclohexylstannyl)-methanamine (15) to purification procedures, it is used crude immediately after workup.
- (23) Moreau, J.; Marchand-Brynaert, J. *Eur. J. Org. Chem.* **2011**, *2011*, 1641–1644.
- (24) Fillmore, C. M.; Kuperwasser, C. *Breast Cancer Res.* **2008**, *10*, R25.
- (25) Chomczynski, P.; Sacchi, N. *Anal. Biochem.* **1987**, *162*, 156–159.
- (26) Schmittgen, T. D.; Livak, K. J. *Nat. Protoc.* **2008**, *3*, 1101–1108.